The University of Southern Mississippi
The Aquila Digital Community

Dissertations

Summer 8-2014

Development and Applications of The Expanded Equivalent Fluid Method

Bharath Kumar Kandula
University of Southern Mississippi

Follow this and additional works at: https://aquila.usm.edu/dissertations

 Part of the Acoustics, Dynamics, and Controls Commons, Applied Mathematics Commons, Other Computer Engineering Commons, and the Physics Commons

Recommended Citation

Kandula, Bharath Kumar, "Development and Applications of The Expanded Equivalent Fluid Method" (2014). *Dissertations*. 293.
https://aquila.usm.edu/dissertations/293

This Dissertation is brought to you for free and open access by The Aquila Digital Community. It has been accepted for inclusion in Dissertations by an authorized administrator of The Aquila Digital Community. For more information, please contact Joshua.Cromwell@usm.edu.

The University of Southern Mississippi

DEVELOPMENT AND APPLICATIONS OF THE EXPANDED EQUIVALENT FLUID METHOD

by

Bharath Kumar Kandula

Abstract of a Dissertation
Submitted to the Graduate School
of The University of Southern Mississippi
in Partial Fulfillment of the Requirements
for the Degree of Doctor of Philosophy

August 2014

ABSTRACT

DEVELOPMENT AND APPLICATIONS OF
THE EXPANDED EQUIVALENT FLUID METHOD

by Bharath Kumar Kandula

August 2014

Ocean acoustics is the study of sound in the oceans. Electromagnetic waves attenuate rapidly in the water medium. Sound is the best means to transmit information underwater. Computational numerical simulations play an important role in ocean acoustics. Simulations of acoustic propagation in the oceans are challenging due to the complexities involved in the ocean environment. Different methods have been developed to simulate underwater sound propagation. The Parabolic-Equation (PE) method is the best choice in several ocean acoustic problems.

In shallow water acoustic experiments, sound loses some of its energy when it interacts with the bottom. An equivalent fluid technique was developed by Zhang and Tindle (ZT) to model sound propagation which is affected by shear in the sea bottom. The reflection coefficient of a soft solid seabed with a low shear speed can be well approximated by replacing the seafloor with a Complex-Density (CD) equivalent fluid of suitably chosen parameters. This is called an equivalent fluid approximation. The ZT method works well in cases where low grazing angles are relevant. This technique was expanded to also perform well in cases where higher grazing angle intervals are relevant. This method is called the Expanded Equivalent Fluid (EEF) method. The EEF method gives an effective CD, $\rho' = \rho'_r + i\rho'_i$, and an effective sound speed in the bottom, c'_p, when a set of bottom parameters (density ρ, sound speed in the bottom c_p, and shear speed c_s) are given as input. The performance of the EEF method has been investigated in several different ocean acoustic environments. Far-field simulations for an array of airgun sources were performed using the CD equivalent fluid parameters. Another application of the EEF method in the geoacoustic inversion process to find an estimate of the elastic bottom parameters of the seafloor was explored. PE broadband simulations were performed to model shear-affected, bottom-interacting sound.

COPYRIGHT BY

BHARATH KUMAR KANDULA

2014

The University of Southern Mississippi

DEVELOPMENT AND APPLICATIONS OF THE EXPANDED EQUIVALENT FLUID METHOD

by

Bharath Kumar Kandula

A Dissertation
Submitted to the Graduate School
of The University of Southern Mississippi
in Partial Fulfillment of the Requirements
for the Degree of Doctor of Philosophy

Approved:

Dr. Michael D. Vera
Committee Chair

Dr. Khin M. Maung

Dr. Ras B. Pandey

Dr. Partha Biswas

Dr. Sungwook Lee

Dr. Maureen Ryan
Dean of the Graduate School

August 2014

ACKNOWLEDGMENTS

I sincerely thank Dr. Michael D. Vera for his guidance and cooperation throughout my graduate career. Most of the knowledge I gained in my graduate career is undoubtedly from Dr.Vera. Working with and learning from Dr.Vera has been a great experience. I thoroughly enjoyed learning ocean acoustics from Dr. Vera. Although I cannot thank him enough for his help, I still would like to convey my sincere thanks to Dr.Vera for guiding me with patience and affection.

The Physics Department Chair, Dr. Khin Maung Maung, has been very supportive and has taken personal care of me in some situations. Many thanks to Dr.Maung.

I would also thank Dr. Stephens for providing very useful information and material during my research. Many thanks to Dr. Hironori Shimoyama for providing valuable information about scientific writing. Special thanks to Dr. Rajendra Timilsina (a former graduate student in the department of Physics, USM) for being a very good friend and for teaching me several helpful tools.

I would like to take this opportunity to thank all other faculty members and graduate students in the department of Physics and Astronomy at USM who have been very friendly and gave valuable suggestions in many situations.

Last but not least, I am thankful for my parents, sister, relatives, and friends who have been supportive and affectionate for all these years.

TABLE OF CONTENTS

LIST OF TABLES

Table

LIST OF ILLUSTRATIONS

Figure

LIST OF ABBREVIATIONS

EEF - Expanded Equivalent Fluid
RAM - Range-dependent Acoustic Modeling
RAMS - Range-dependent Acoustic Modeling with Shear
OASES - Ocean Acoustics and Seismic Exploration Synthesis
PE - Parabolic Equation
CD - Complex Density
PERAM - Parabolic Equation Range-dependent Acoustic Modeling
CTD - Conductivity Temparature Density
SSP - Sound Speed Profile
BASSEX - Basin Acoustic Seamount Scattering Experiment
NPAL - North Pacific Acoustic Laboratory
ATOC - Acoustic Thermometry of Ocean Climate
AET - Acoustic Engineering Test
TL - Transmission Loss
BL - Bottom Loss

Chapter I
INTRODUCTION

I.1 Ocean Acoustics

Inquisitiveness has driven scientific exploration to the edge of our solar system and beyond. But probably the least explored areas on Earth are oceans. Scientists predict that there are more than a million different animal and plant species living in the oceans [8]. Most of them are undocumented. Sound waves are well-suited to communicate underwater and to understand the state of the ocean and the life of beings in it.

Acoustics has been one of the fundamental areas of Physics. It has become a much broader and more interdisciplinary subject since the beginning of the twentieth century. The primary purpose of acoustics is to communicate. Sound is a longitudinal pressure wave; vibrations of the particles are parallel to the direction of the wave propagation. Sound requires a medium to travel. Sound transmits information through the medium. Its propagation involves compressions and rarefactions of the particles of the medium. The sound speed (c) is different in different media due to differences in mechanical properties. Speed of sound at 1 atm pressure in various materials is given below.

The speed of sound in air at 20°C is 343 m/s. In water at 25°C it is 1493 m/s, in seawater at 25° it is 1533 m/s, and in Aluminium at 0°C it is 5100 m/s [9]. Amplitude, frequency, and wavelength are the basic parameters of a sound wave. Loudness of a sound wave is measured using the decibel (dB) scale.

Ocean acoustics is the study of propagation of sound in the sea. Study of sound propagation in the oceans has been going on for more than five centuries. Sound is the dominant means of transmitting information in the ocean environment. As the sound wave travels through the ocean, it is affected by the conditions of the ocean medium [10]. So, analyzing the received sound can provide information about the medium. Seventy one percent of Earth's surface is occupied by oceans. Therefore, attempts to understand global weather, life of creatures underwater, phenomena like volcanic activity under the sea, and the dynamics of tsunamis depend upon knowledge of the oceans.

To use sound as a tool in the ocean environment, the following phenomena must be understood: the speed of sound, sound attenuation, refraction, how sound bends around objects

and into shadows, and the way sound reflects, scatters and transmits at boundaries. All these phenomena depend on physical characteristics of the ocean volume, surface, and bottom [11].

The sea surface and bottom are the two boundaries in an ocean environment. Marine biology, geology, and physical oceanography studies are pursued using shallow water acoustic techniques. Bottom interaction of the sound should be taken into account for the shallow water case. In deep water, acoustic interaction with the boundaries is less important. The deep water environment is significantly different compared to shallow water. The surface boundary has been well studied and is straightforward to model, but the bottom boundary is more complicated and has been a challenge in many cases. Another major factor is the thermal variation between deep and shallow water. The speed of sound in shallow water is dictated mainly by temperature and by pressure in deep water.

The sound frequency range that a human ear can recognize is roughly 20 Hz to 20 kHz. But ocean acoustics covers a much wider range. The approximate ocean acoustics range is from 1 Hz to 300 kHz. The sound speed in water is approximately 1500 m/s. So the acoustic wavelengths range from 5×10^{-3} m to 1500 m in this frequency interval [10].

I.1.1 Underwater Acoustics Applications

Underwater acoustics has various applications. These applications are in detection, tracking, imaging, communication, and measurement. Although there are many complexities imposed by the environment, underwater acoustics has been the tool that best answers present needs. The study of life underwater, ocean acoustic tomography (a process used to measure the state of the ocean), and oil exploration and many more applications are possible due to the development in underwater acoustic technology. Measurement of ocean interior structure and thermometry by acoustic tomography is useful to understand climate change [2]. Some of the modern applications of underwater acoustics are briefly discussed below.

• *SONAR (SOund Navigation And Ranging)*: SONAR is useful in detecting and identifying underwater objects such as submarines. SONAR devices are used to estimate the range between the sonar and its targets and also find the speed and location of the target.

• *Bathymetric echosounders*: Echosounders are also known as fathometers. These are special sonar used to measure the depth of a water column.

• *Fishery sounders*: These are used for the detection and localization of fish shoals. Fishery sounders are similar to bathymetric sounders.

• *Sidescan sonar*: These devices are used to obtain high-definition acoustic imaging of the seafloor. Signals transmitted by a sidescan sonar sweep the ocean bottom. The reflected signals

provide an image of bottom irregularities, obstacles, and structure of the seabed. Sidescan sonars are used in marine geology.

• *Sediment profilers*: Multi-layered internal structure of the seafloor can be analyzed using sediment profilers. The frequency used by these devices is much lower, which allows the signal to penetrate deep into the seabed. Sediment profilers are used in oil and gas exploration, as well as in geophysics.

• *Acoustic communication systems*: These systems are used to communicate digital data underwater. Examples include sending remote control commands, transmitting images, or data results.

• *Positioning systems*: These are used to track underwater autonomous vehicles. The mobile targets are located by measuring the time delays of the several signals coming from the transmitters attached to those devices.

• *Ocean acoustic tomography networks*: These networks measure the sound propagation times (over large distances) from a sound source to receivers. These experiments are useful to estimate ocean temperatures.

There is an increase of acoustic pollution due to human activity. Sources include ship noise, offshore industry, and coastal activity. The global increase in underwater noise levels could harm marine life and the environment. Marine bioacoustics research may provide scientific insight on these issues and is also useful to understand communication of marine life [12].

I.2 Speed of Sound in the Ocean Environment

As mentioned before, sound speed varies for different media. The speed of sound c in water is about five times faster than its speed in air. The sound speed in air at sea level at 15°C is 340 m/s and in the ocean it ranges from 1450 m/s to 1540 m/s. From this it is clear that sound speed variations in the ocean are relatively small, but small changes of c significantly impact sound transmission in the ocean [13]. Sound speed in the ocean is a function of temperature T, salinity S, and hydro static pressure P. Sound speed increases with increases in any of these three quantities. Sound speed dependence on temperature and pressure is much stronger than salinity. Variation of sound speed with depth in the ocean results in a sound speed profile (SSP). Sound speed as a function of ocean depth z is denoted as $c(z)$.

The ocean surface is warmed due to solar heating. The surface temperature varies depending on the geographic location, time and season. As we go below the surface of the ocean for the first few hundred meters, temperature rapidly decreases. At depths beyond 1000 m, the variation

of temperature is less important. The region of depth in which temperature decreases in the ocean is called the thermocline. A deep, nearly isothermal layer exists below the thermocline. These are colder deep-water layers [14]. Hydrostatic pressure starts dominating in the deep ocean regions. Sound speed increases linearly with increase in pressure.

Measurement of c can be done directly either using velocimeters or by empirical formulae if the temperature, salinity, and pressure (or depth) are known. An empirical equation to measure c is given below. It is a function of three independent variables T in °C, S in parts per thousand and depth Z in meters [13].

$$c = 1449.2 + 4.6T - 0.055T^2 + 0.00029T^3 + (1.34 - 0.010T)(S-35) + 0.016Z. \quad \text{(I.1)}$$

A more sophisticated standard equation to calculate the speed of sound called NRL II is

$$c_{STP} = c_{000} + \Delta c_T + \Delta c_S + \Delta c_P + \Delta c_{STP} \quad \text{(I.2)}$$

where

$$\begin{aligned}
c_{000} &= 1402.392 \\
\Delta c_T &= 0.501109398873 \times 10^1 T - 0.550946843172 \times 10^{-1} T^2 + 0.221535969240 \times 10^{-3} T^3 \\
\Delta c_s &= 0.132952290781 \times 10^1 S + 0.128955756844 \times 10^{-3} S^2 \\
\Delta c_P &= 0.156059257041 \times 10^0 P + 0.244998688441 \times 10^{-4} p^2 \\
&\quad -0.883392332513 \times 10^{-8} P^3 \\
\Delta c_{STP} &= -0.127562783426 \times 10^{-1} TS + 0.635191613389 \times 10^{-2} TP \\
&\quad +0.265484716608 \times 10^{-7} T^2 P^2 - 0.159349479045 \times 10^{-5} TP^2 \\
&\quad +0.522116437235 \times 10^{-9} TP^3 - 0.438031096213 \times 10^{-6} T^3 P \\
&\quad -0.161674495909 \times 10^{-8} S^2 P^2 + 0.968403156410 \times 10^{-4} T^2 S \\
&\quad +0.485639620015 \times 10^{-5} TS^2 P - 0.340597039004 \times 10^{-3} TSP
\end{aligned}$$

T is in degrees Celsius, S is in parts per thousand, and P is in kilograms per square centimeter gauge. The NRL II equation has a standard deviation of 0.05 m/s [15].

The Munk Canonical sound speed profile is an analytic model shown in Figure I.1. It is intended to capture the basic features of sound speed variation with depth. It has the following

form:

$$c(Z) = c_{axis}[1 + \varepsilon(e^{\eta} - \eta - 1)] \tag{I.3}$$
$$\eta = 2(Z - Z_{axis})/B$$

The parameters used are $\varepsilon = 5.7 \times 10^{-3}$, $c_{axis} = 1490$ m/s, $Z_{axis} = -1000$ m, and $B = 1000$ m [16].

An example of ray paths with three different launch angles is shown in Figure I.2. These rays are launched from the sound channel axis, the depth where the speed of sound is minimum. The ray with launch angle -10° travels deeper into the water and therefore propagates faster than rays with -6° launch angle.

I.2.1 Snell's Law

SOFAR stands for SOund Fixing And Ranging. The sound speed inside the ocean is minimum at a depth of around 1000 m but this value varies depending on the geographical location. A horizontal layer of water in the ocean where the sound speed is minimum is called the SOFAR axis or the deep sound channel. This sound channel was first discovered by Ewing and Worzel in 1948 [3]. Discovery of this underwater sound channel has made long range propagations possible. Sound rays transmitted from the deep sound channel tend to refract toward layers with smaller sound speed (due to Snell's law) and propagate thousands of kilometers without touching the ocean surface or bottom [17].

Consider medium one with refractive index n_1 and wave speed c_1 and medium two with refractive index n_2 and wave speed c_2. Snell's law states that the ratio of the cosine of the angle of incidence ϕ_1 to angle of refraction ϕ_2 (ϕ_1 and ϕ_2 are relative to horizontal in medium 1 and 2 respectively) is equal to the ratio of the wave speeds of the two media. Figure I.3 shows incident and refracted rays with corresponding angles.

$$\begin{aligned} c_1 \cos\phi_2 &= c_2 \cos\phi_1 \\ \frac{\cos\phi_1}{c_1} &= \frac{\cos\phi_2}{c_2} \\ \frac{\cos\phi}{c} &= \text{constant} \end{aligned} \tag{I.4}$$

ϕ is the angle between the ray and the surface or boundary of the two media. In optics, angles of incidence, and refraction are usually denoted relative to normal, which would be

vertical in this case. But in ocean acoustics it is convenient to indicate incident and refraction angles relative to horizontal. Ocean medium consists of many layers of water with different sound speeds. So cosine of the angle ϕ is considered. c is a reference sound speed in the medium.

Snell's law governs the refraction of the sound rays underwater. According to the law the sound rays bend or refract toward the medium of lower sound speed. The value of $\frac{\cos\phi}{c}$ is the same anywhere in the ray path.

I.3 Shear in the Sea Bottom

It is known that the sea bottom is a solid and supports compressional and shear waves. When a sound wave incident on a solid from a fluid, it will produce three waves (a reflected wave into the same fluid medium, a refracted compressional sound wave, and a transverse shear wave in the solid). Both the refracted sound and the shear waves in the bottom result in loss, a reduction in the energy of the sound reflected back into the fluid. θ_z is the grazing angle between incident wave and the surface as shown in Figure I.4. The incident sound wave causes stress on the solid and due to the elastic restoring force in solids, transverse shear waves will be produced. The speed of these waves is less than the speed of sound waves. Shear waves are not possible in liquids since liquids lack this shearing property [18].

I.3.1 Summary

This dissertation is structured as follows:

In Chapter II, background in theoretical methods is presented. The use of equivalent fluids in ocean acoustic simulations where bottom interactions are present is discussed in Chapter III. This chapter also explains the development of the expanded equivalent fluid (EEF) method and its application to different environments. The far-field simulation of sound from an array of airgun sources is presented in Chapter IV. An application of the EEF method based on the Basin Acoustic Seamount Scattering Experiment (BASSEX) is shown in Chapter V. Finally, there is a summary of the entire work in the Chapter VI.

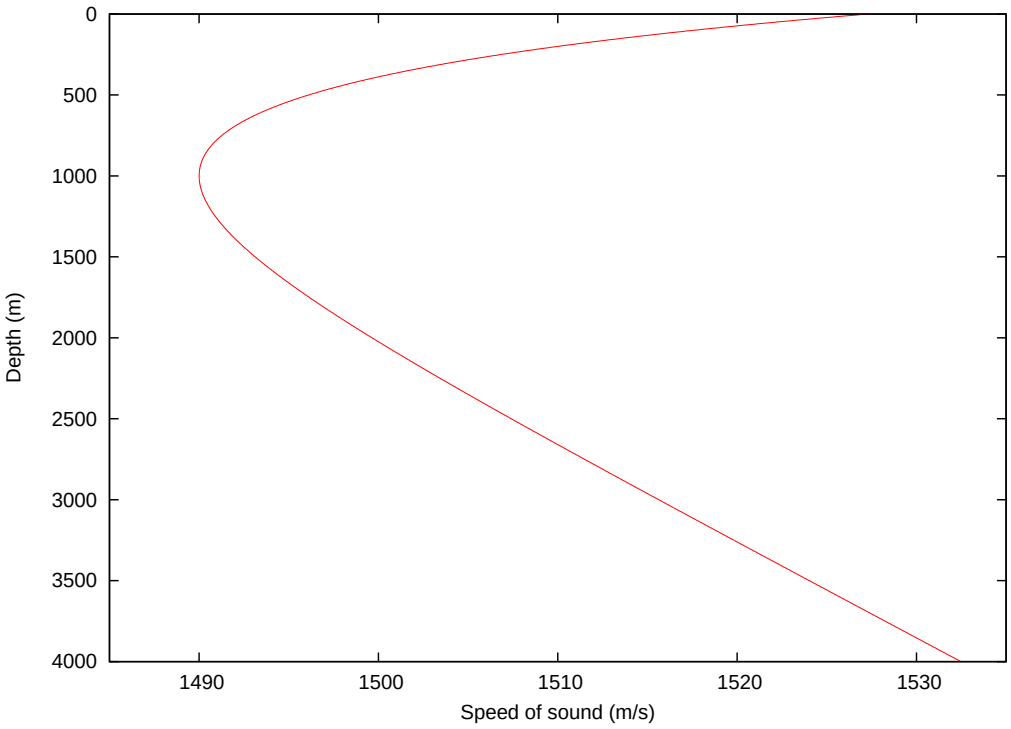

Figure I.1: A canonical sound speed profile showing the variation of sound speed with depth up to 4000 m. This is an analytic model given by Equation I.3.

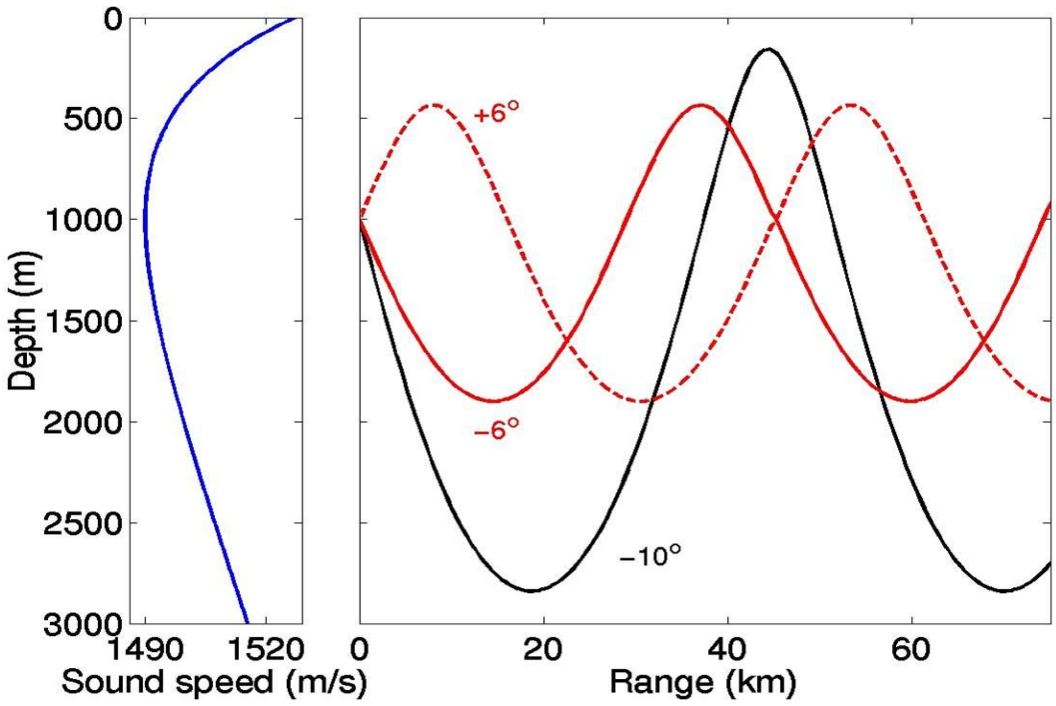

Figure I.2: Ray paths using the SSP in the left panel are shown. Sample rays launched from a depth of 1000 m at three different initial launch angles ($+6^\circ$, -6°, and -10°) are depicted. This picture was taken from "Examples and applications in long-range ocean acoustics" by M D Vera [2].

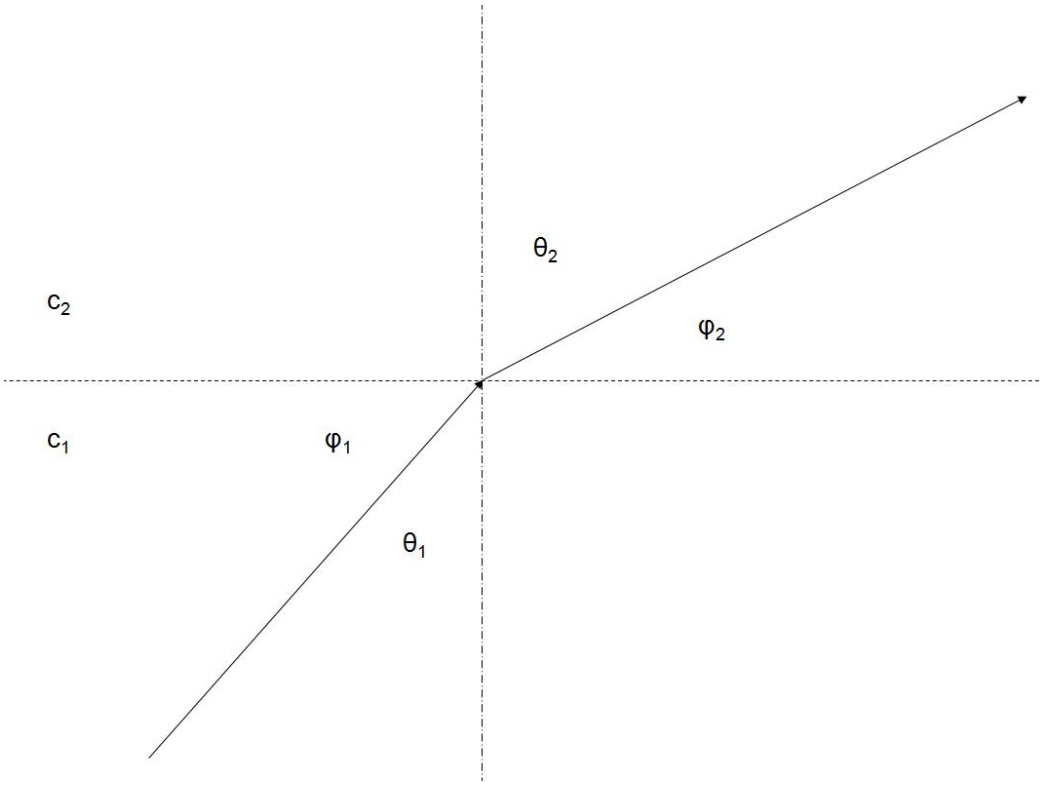

Figure I.3: This is a depiction of two discrete layers with sound speeds c_1 and c_2. This figure shows the incident and refracted rays and the corresponding angles. ϕ_1 and ϕ_2 are the incident and refracted angles relative to horizontal respectively. This picture was taken from "Examples and applications in long-range ocean acoustics" by M D Vera [2].

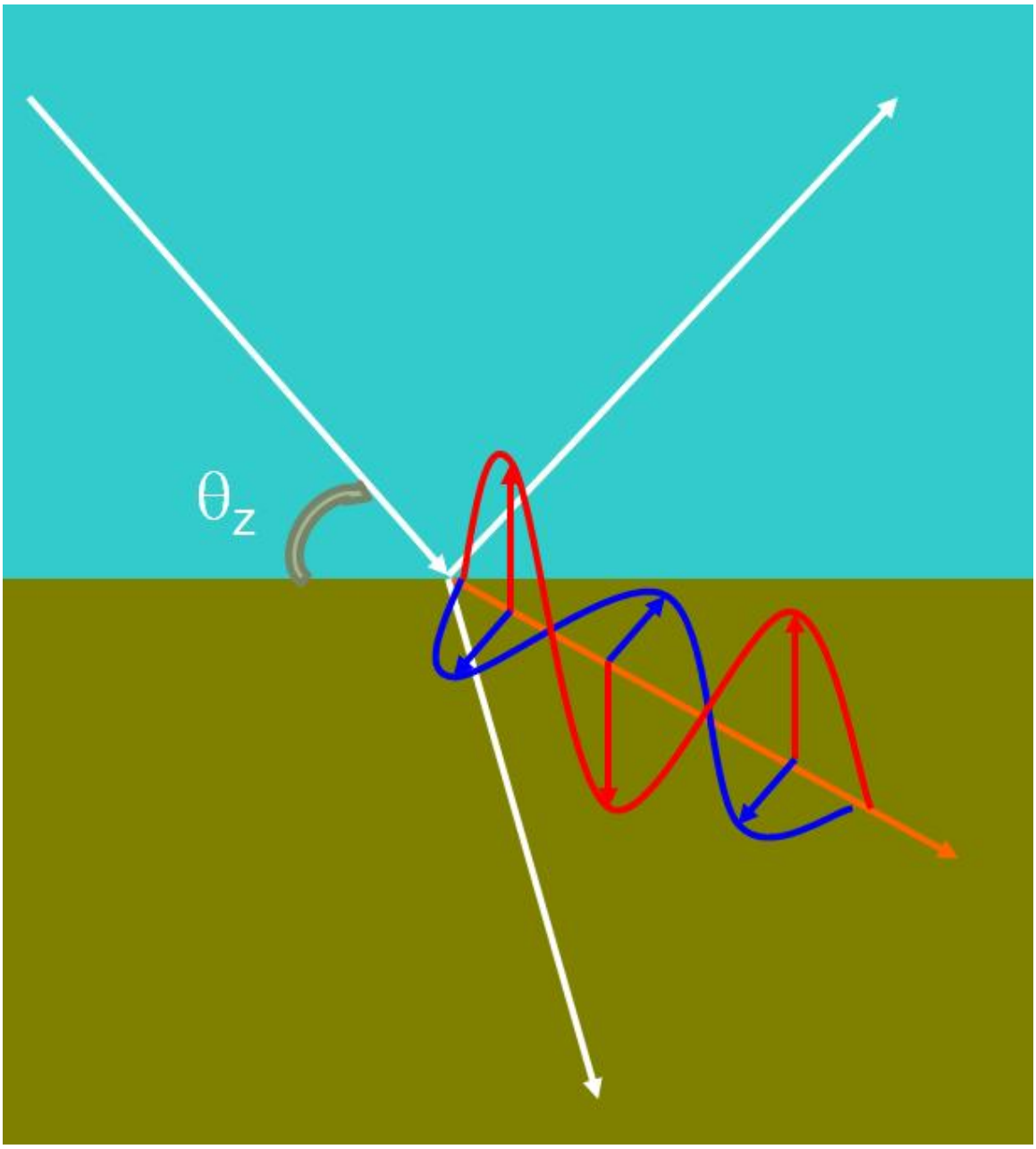

Figure I.4: This figure shows the incident ray, reflected ray, refracted ray, and shear waves in the sea bottom. Notice that the shear waves are transverse (displacements of the particles are perpendicular to the direction of propagation of the wave). θ_z is the grazing angle between incident ray and the interface.

Chapter II

BACKGROUND

II.1 A Brief Literature Survey

Numerical simulations play an important role in ocean acoustics. Ocean acoustic simulations involve large-scale scientific computations. The environmental parameters of the ocean are highly variable; this makes the simulations more complex. Ocean acousticians and scientists have developed solutions to simple ocean acoustic problems and then extended those solutions to cover challenging problems. Existing methods are powerful, but they are still limited. Some approximations have to be considered to get acceptable results for real-world environmental conditions [19].

Ocean acoustic experiments require extensive machinery, manpower, and time. Computer simulations are a big advantage for ocean acoustic experiments. In most cases, the main goal in ocean acoustic simulations is to obtain a desired acoustic signal which closely approximates the signal received in experiments. This aids in the analysis of the experimental results. Some of the challenges in achieving this goal are constructing an environment that is close to realistic conditions, implementing boundary conditions and identifying an appropriate sound speed profile (SSP).

In shallow water simulations, sound waves which repeatedly bounce from the seabed over long ranges would largely attenuate and die out [20]. If sound waves only bounced a few times from the seabed, they would lose some of their energy. This is called bottom loss. In shallow water cases, computational modeling is much more challenging, since the received sound signal suffers energy loss due to the seafloor interaction. Equivalent fluids can be used to model the sound that has interacted with the seafloor [21].

II.2 Computational Modeling of Underwater Acoustics

The standard Helmholtz wave equation is used to mathematically describe sound propagation in the ocean. The standard form of the wave equation for pressure is

$$\nabla^2 p - \frac{1}{c^2}\frac{\partial^2 p}{\partial t^2} = 0 \tag{II.1}$$

where $p(x,t)$ is the acoustic pressure, c in the wave equation represents the speed of sound, and ∇^2 is the Laplacian operator.

The solution for the wave equation in one dimension in terms of a sinusoidal plane wave is

$$p(x,t) = p_0 \sin\left(\frac{2\pi x}{\lambda} - 2\pi f t + \phi\right) \tag{II.2}$$

where p_0 is the amplitude of the pressure disturbance, f is the frequency, λ is the wavelength, T is the time period, and ϕ is the phase shift. The phase speed is given by $c = f\lambda$. The term $\frac{2\pi}{\lambda}$ is the angular wave number k, and $2\pi f$ is the angular frequency ω. The speed can be written as $c = \frac{\omega}{k}$. The solution can be rewritten as

$$p(x,t) = p_0 \sin(kx - \omega t + \phi) \tag{II.3}$$

The argument of the sine function $(kx - \omega t + \phi)$ represents the phase [3].

Sound propagation in water is affected by the sound speed profile (SSP). So the SSP, the boundary conditions, and the environmental parameters must be known to find a numerical solution to the wave equation.

There are five types of models available to solve the wave equation. Each model has its advantages and disadvantages. Experts choose a suitable model based on their environment and desired goals. The five types of models for acoustic propagation in the ocean are spectral or fast field program (FFP), normal mode (NM), ray, and parabolic equation (PE) models, and direct finite-difference (FD) or finite-element (FE) solutions of the full wave equation. All of these models allow the variation of the ocean environment with ocean depth. There are cases where the ocean bottom strongly varies with range [22] or the SSP varies with range. These environments are called range-dependent. FFP and NM models are used in range-independent environments. PE, ray, FD or FE are useful to model sound propagation in range-dependent environments. In general, ray theory is especially useful for high frequencies and other models are preferred at low frequencies (less than a kilohertz) [23].

When a sound wave propagates in the ocean, it suffers energy loss due to different mechanisms. Those are mainly dominated by absorption, bottom reflection, and surface, spreading, and volume scattering loss.

II.2.1 Transmission Loss

Transmission loss (TL) is a standard measure of the change in underwater acoustic signal strength with range. It is defined as the ratio of the acoustic intensity $I(r,z)$, or pressure squared

$P^2(r,z)$, at a field point to the reference intensity I_0 at 1 m distance from the source. Transmission loss is measured in decibels (dB) as a function of range. Transmission loss (dB re 1 m) is the sum of a loss due to geometrical spreading and a loss due to attenuation [23].

$$TL = -10\log\frac{I(r,z)}{I_0} \tag{II.4}$$

$$TL = -20\log\frac{|P(r,z)|}{|P_0|} \tag{II.5}$$

II.2.2 Bottom Loss

When sound interacts with the sea bottom, some of its energy goes into the seafloor and produces compressional and shear waves. The amount of acoustic energy lost in bottom interaction is called bottom loss. This loss depends on the roughness of the sea bottom and the material properties of the bottom. Bottom loss significantly impacts long-range propagation in shallow water. Information about the seafloor material properties must be known to model the sound that has interacted with the seafloor. Those properties include the compressional wave speed c_p (sound speed in the sea bottom), the shear wave speed c_s, the compressional wave attenuation α_p, the shear wave attenuation α_s, and the density ρ. If the seafloor has a negligible amount of sediment overlying the basement, then the bottom is considered as elastic for modeling purposes. An elastic bottom supports both compressional and shear waves. In reality, the seafloor exhibits both viscous and elastic characteristics [23].

Bottom loss (BL) is measured in decibels (dB) as a function of grazing angle θ_z. The expression to measure the value of bottom loss is shown below.

$$BL = -10\log\left|V_{fs}\right|^2 \tag{II.6}$$

where V_{fs} is the reflection coefficient for plane waves incident on the fluid-solid interface.

$$V_{fs}(k) = \frac{\gamma_1[\frac{\rho_2 P(k)}{\rho_1}] - i\eta_2}{\gamma_1[\frac{\rho_2 P(k)}{\rho_1}] + i\eta_2} \tag{II.7}$$

$$k = \frac{\omega}{c_1}\cos\theta_z \tag{II.8}$$

ρ_1, ρ_2 are the densities of a homogeneous fluid and solid respectively. γ_1 and $i\eta_2$ are the vertical wave numbers in the fluid and solid respectively. The parameter k is the horizontal wave number, θ_z is the grazing angle between the incident wave and the boundary, and ω is the angular

frequency. The parameter $P(k)$ characterizes the acoustic effect of elastic shear and is explained in Chapter III with some detail.

II.2.3 Attenuation of sound in seawater

When sound travels through the ocean, some of its energy continuously attenuates due to absorption, which means the sound energy is transformed into heat. Scattering of the sound due to different types of inhomogenities in the ocean also causes sound attenuation in seawater.

The frequency dependence of the attenuation of sound in seawater is given by the following simplified expression

$$\alpha' \simeq 3.3 \times 10^{-3} + \frac{0.11 f^2}{1+f^2} + \frac{44 f^2}{4100+f^2} + 3.0 \times 10^{-4} f^2 [dB/km] \tag{II.9}$$

The frequency f should be considered in kHz in the expression. α' is the attenuation of sound in seawater. α' has some dependence on pressure, temperature, salinity, and acidity (pH value). Equation II.9 is sufficiently accurate for most problems in ocean acoustics even though it does not consider the dependence of α' on some quantities (P,T,S, and pH). This expression applies for a temperature of 4° C, a salinity of 35 ppt, a pH of 8.0, and a depth of about 1000 m.

The frequency dependence of α' is roughly divided into four regimes. In the lowest frequency regime (up to 50 Hz), region 1, the mechanism is related to leakage out of the deep sound channel. In regions 2 (f between 50-1500 Hz) and 3 (1.5-150 kHz), attenuation is due to chemical relaxations of boric acid $B(OH_3)$ and magnesium sulphate $MgSO_4$ respectively. Region 4 (f higher than 150 kHz) is dominated by the shear and bulk viscosity associated with salt water.

From Equation II.9, it is clear that attenuation is very small for low-frequency sound in seawater. Although attenuation of sound increases with increase in frequency, no other kind of radiation competes with sound waves for long-range propagation in the ocean [23].

II.2.4 Ray Simulations

Ray theory is a quite effective method for understanding the sound propagation at high frequencies in inhomogeneous media like the ocean [13]. Ray simulations have been very popular for many years in underwater acoustics. Rays are perpendicular to wavefronts (surfaces of constant phase) and point toward the wave propagation direction (see Figure II.1). Ray paths provide travel times and the propagation direction of sound energy. Ray theory is mainly used for the study of sound in deep water or at high frequency. In some cases, it can be used in low

and mid-frequency shallow water sound propagation [24]. Refraction of rays through different layers with varying propagation speeds is governed by Snell's law.

Ray theory is based on the "eikonal equation." The equation is derived from the wave equation by assuming a solution of the following form.

$$p(\mathbf{r}) = A(\mathbf{r})e^{i(k_0 W(\mathbf{r})-\omega t)} \tag{II.10}$$

p and A are functions of the position vector r, ω is the angular frequency, and $k_0 = \frac{\omega}{c_0} = \frac{2\pi}{\lambda_0}$ is a reference wave number. c_0 and λ_0 are the reference propagation speed and wavelength respectively. $W(\mathbf{r})$ is the eikonal, which contains the spatial dependence of the wave phase [25].

By substituting the wave solution, the wave equation (Equation II.1) gives,

$$\nabla^2 A - k_0^2 A|\nabla W|^2 + \frac{\omega^2}{c^2}A + 2ik_0\nabla A\cdot\nabla W + ik_0 A\nabla^2 W = 0 \tag{II.11}$$

The real part of the equation can be written as

$$|\nabla W|^2 - \frac{\omega^2}{k_0^2 c^2} = \frac{\nabla^2 A}{k_0^2 A} = \frac{\lambda_0^2\nabla^2 A}{4\pi^2 A} \tag{II.12}$$

where $c_0^2 = \frac{\omega^2}{k_0^2}$.

If the right hand side of the above equation is small (function A is not strong and λ_0 is small), then the above equation becomes

$$\begin{gathered} |\nabla W|^2 - \left(\frac{c_0^2}{c^2}\right) = 0 \\ |\nabla W|^2 = \left(\frac{c_0^2}{c^2}\right) \\ |\nabla W|^2 = n^2 \end{gathered} \tag{II.13}$$

Where $n^2 = \frac{c_0^2}{c^2}$. n is the index of refraction. Equation II.13 is known as the eikonal equation. Surfaces of constant W are wavefronts, so the gradient of W (which is ∇W) indicates the direction of ray propagation. According to Equation II.13, the magnitude of ∇W is equal to the index of refraction. From this, $\nabla W = n\hat{l}$. Where $\hat{l}$ is a unit vector in the ray direction. The derivative of ∇W along the ray direction is shown below.

$$\frac{d}{dl}(\nabla W) = \hat{l}\cdot\nabla(\nabla W) \tag{II.14}$$

Using $\nabla W = n\hat{l}$,

$$\frac{d}{dl}(\nabla W) = \frac{\nabla W}{n} \cdot \nabla(\nabla W) \tag{II.15}$$

Differentiating Equation II.13,

$$\begin{aligned} \nabla(\nabla W)^2 &= 2\nabla W \cdot \nabla(\nabla W) \\ \nabla(n^2) &= 2n\nabla n \\ \nabla W.\nabla(\nabla W) &= n\nabla n \end{aligned} \tag{II.16}$$

Since $\nabla W = n\hat{l}$ and using equation II.16, Equation II.15 can be expressed as

$$\frac{d}{dl}(n\hat{l}) = \nabla n \tag{II.17}$$

Equation II.17 governs ray propagation in a variable medium. Consider ray propagation within the xz plane where $n(\mathbf{r}) = n(z)$. If θ is the angle between the vertical and the ray direction, then $\hat{l} = \sin\theta\hat{x} + \cos\theta\hat{z}$. The x component of Equation II.17 is $\frac{d}{dl}(n\sin\theta) = 0$. That is $n\sin\theta$ =constant. This is Snell's law [2].

In Equation II.10, if the phase is equated to a constant at a particular time (t_0), then $W(\mathbf{r})$ is written as

$$\omega t_0 - k_0 W = \text{constant}$$

$$W(\mathbf{r}) = \frac{\omega t_0 - \text{constant}}{k_0} \tag{II.18}$$

The eikonal $W(\mathbf{r})$ describes a surface in space [3].

Snell's law: In ocean acoustics, the ray equations can be phrased in terms of a Hamiltonian system using range (r) as the independent variable. The conjugate position and momentum are z and $p = \frac{\sin\theta}{c}$ (θ is measured relative to horizontal) respectively.

$$\begin{aligned} H &= -(c^{-2} - p^2)^{1/2} \\ \frac{dz}{dr} &= \frac{\partial H}{\partial p} \\ \frac{dp}{dr} &= -\frac{\partial H}{\partial z} \end{aligned} \tag{II.19}$$

From the above system of equations, the Hamiltonian can be written as

$$\begin{aligned} H &= -(c^{-2} - p^2)^{1/2} \\ H &= -\left(\frac{1}{c^2} - \frac{\sin^2\theta}{c^2}\right)^{1/2} \\ H &= -\left(\frac{\cos^2\theta}{c^2}\right)^{1/2} \\ H &= -\frac{\cos\theta}{c} \end{aligned} \tag{II.20}$$

Snell's law says that $\frac{\cos\theta}{c}$ is constant everywhere in the ray path. So from the above equation, the conservation of the Hamiltonian is Snell's law.

Using the expression of conjugate momentum and performing the partial differentiation, the expressions in Equation II.19 can be stated as

$$\frac{dz}{dr} = \tan\theta \tag{II.21}$$

$$\frac{dp}{dr} = \frac{-\frac{\partial c}{\partial z}}{c^2(1-(pc)^2)^{1/2}} \tag{II.22}$$

and travel time (t) can be expressed as

$$\frac{dt}{dr} = \frac{1}{c(1-(pc)^2)^{1/2}} \tag{II.23}$$

The above Equations II.19 and II.23 can be treated using numerical methods such as Runge-Kutta integration. The solutions give a high-frequency estimate of the nature of the propagating wave [25].

II.2.5 Parabolic-Equation (PE) Simulations

A parabolic-equation model can be used to simulate the propagation of sound on a two-dimensional plane of range and depth. The parabolic approximation converts an elliptic equation which has second order derivatives in both range and depth into a parabolic equation with one of the derivatives having only first order. This approximation assumes a dominant propagation direction. This approach is useful in ocean acoustics since propagation is dominated by near-horizontal angles. An elliptic wave equation can be written as

$$\nabla^2 p + k^2 p = 0 \tag{II.24}$$

Consider wave travel mainly in the x direction. This equation can be rewritten as

$$[\nabla_T^2 + \partial_{xx} + k^2]p = 0 \tag{II.25}$$

where ∇_T^2 contains the second order partial derivatives transverse to the propagation direction. That is, $\nabla_T^2 = \partial_{yy} + \partial_{zz}$. The spatial deviation of the wave from horizontal plane wave propagation can be separated explicitly with $p = \psi(\mathbf{r})e^{ik_0 x}$.

The terms in the Equation II.25 can be written as

$$\begin{aligned} \nabla_T^2 p &= e^{ik_0 x}\nabla_T^2 \psi \\ \partial_{xx} p &= [\partial_{xx}\psi + 2ik_0\partial_x\psi - k_0^2\psi]e^{ik_0 x} \end{aligned} \tag{II.26}$$

Using the above equations, Equation II.25 becomes

$$\nabla_T^2 \psi + [\partial_{xx}\psi + 2ik_0\partial_x\psi] + (k^2 - k_0^2)\psi = 0 \tag{II.27}$$

If ψ is expressed as $\exp[i(k_x - k_0)x + k_y y + k_z z]$ then $\partial_{xx}\psi = i(k_x - k_0)\partial_x\psi$. For the variations in ocean sound speed and the relevant angles, $|k_x - k_0|$ is small compared to k_0. So the second derivative term $\partial_{xx}\psi$ can be neglected compared to the first derivative term in Equation II.27.

Now, the standard parabolic equation for sound propagation [26, 25] from Equation II.27 can be stated as

$$2ik_0\partial_x\psi = -\nabla_T^2\psi + (k_0^2 - k^2)\psi \tag{II.28}$$

There are many different parabolic approximations to the elliptic wave equation. Equation II.28 is the standard narrow-angle equation. It is accurate only for 10°-15° propagation angles

off the horizontal. However, wide-angle equations have been derived and numerically solved previously. These are based on an operator formalism. The wave equation is

$$P\psi = ik_0(Q-1)\psi \tag{II.29}$$

$$\frac{\partial \psi}{\partial r} = ik_0\left(\sqrt{\left(n^2 + \frac{1}{k_0^2}\frac{\partial^2}{\partial z^2}\right)} - 1\right)\psi \tag{II.30}$$

In the above equation, $P = \frac{\partial}{\partial r}$. $Q = (1+q)^{1/2}$ is the square-root operator. Where

$$q = \varepsilon + \mu, \quad \varepsilon = n^2 - 1, \quad \mu = \frac{1}{k_0^2}\frac{\partial^2}{\partial z^2} \tag{II.31}$$

Using a Taylor expansion for the operator Q, a solvable wave equation can be written as

$$\frac{\partial \psi}{\partial r} = \frac{ik_0}{2}\left(n^2 - 1 + \frac{1}{k_0^2}\frac{\partial^2}{\partial z^2}\right)\psi \tag{II.32}$$

Using rational-function approximations to the square-root operator Q, PE approximations can be obtained that are valid for wider angles. A general form of these approximations is

$$\sqrt{1+q} \simeq \frac{a_0 + a_1 q}{b_0 + b_1 q} \tag{II.33}$$

a_0, a_1, b_0, and b_1 are coefficients. Different sets of coefficients can be chosen to minimize error over a given angle interval [23]. The rational-function representation shown in the above equation gives a good accuracy for propagation angles below $\pm 40^\circ$. Using different rational-function representations for the Q, a more wide-angled PE approximations were derived. A more wide-angled PE (accurate to $\pm 55^\circ$) based on a Padé series expansion was first implemented by Collins [27, 28]. PE approximations can also be used for elastic media. An elastic PE has been successfully implemented by Collins, Wetton, and Brooke [29, 30].

A computer code known as RAM (Range-dependent Acoustic Modeling) was developed by Michael D. Collins. It is a FORTRAN code based on the parabolic equation (PE) method. The PE method is very efficient for range-dependent acoustic modeling. A Split-step Padé solution is used in RAM to allow large range steps. Acoustic parameters vary with range in range-dependent environments. An energy-conservation correction is applied to accurately handle the range-dependence. In this method, the numerical solution of the PE is achieved by repeatedly solving tridiagonal systems of equations [31].

RAMS (Range-dependent Acoustic Modeling with Shear) was implemented to compute the effects of shear. It is often complicated to simulate a range-dependent broadband long-range transmission using RAMS [31]. The reasons are numerical instability, poorly defined computational grid requirements, and an inability to handle steep bottom slopes. However, RAMS can accurately simulate transmissions for a single frequency. RAMS single frequency simulation was used as a benchmark result in a few examples in Chapter III.

A sample ray simulation and a broadband PE simulation are shown in Figures II.2 and II.3 respectively. Propagation of rays and wavefronts for a range of 1000 km is modeled. The source depth is taken as 1000 m. A canonical sound speed profile is used in both cases (See Figure I.1 in Chapter I). In Figure II.2, several dots make those rayfronts. Each dot in a rayfront indicates a ray arrival at the receiver at a specified range. Similarly, Figure II.3 depicts the acoustic intensity from a PE simulation at 1000 km for the same environment conditions.

II.3 Ocean Acoustics and Seismic Exploration Synthesis (OASES)

OASES is a benchmark computer code used to model seismo-acoustic propagation using wavenumber integration technique. OASES was developed by Henrik Schmidt. It is an upgraded version of SAFARI (Seismo-Acoustic Fast-field Algorithm for Range-independent environments). It is a direct, global matrix approach. It provides numerical efficiency and stability over SAFARI.

OASES is useful to model sound propagation in range-independent environments. In Chapter III, OASES is used to model single frequency sound to compare transmission loss curves for convergence testing.

The wavenumber integration approach is a numerical implementation of the integral transform technique for horizontally stratified (layered) media. The wavenumber integration approach is not only applied to homogeneous fluid layers but also extended to treat cases with depth-dependent sound speed and elastic layers as well. The wave field in each layer is represented by a superposition of the field produced by a random number of sources and an unknown field satisfying homogeneous wave equations. Boundary conditions satisfied at all interfaces are used to determine these unknown fields. The local boundary conditions at each interface are expressed as a linear system of equations in the Hankel transforms of the potentials in the adjacent layers. These local systems of equations are combined in a global system of equations expressing the boundary conditions at all interfaces. The field in all layers can be obtained simultaneously using the numerical solution of the global system of equations [23].

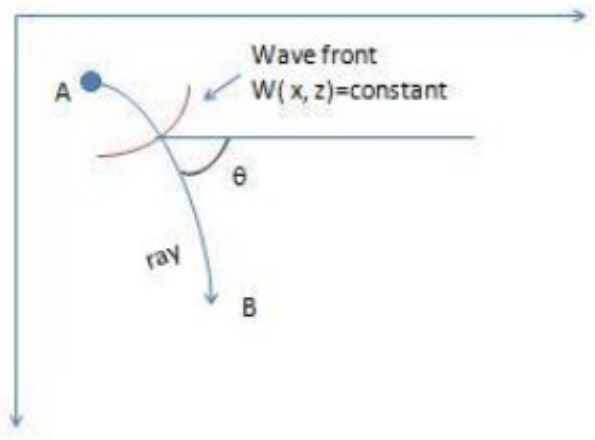

Figure II.1: The figure shows a ray path pointing perpendicular to the wavefront (a surface of constant phase). The ray path indicates the direction of the propagation of energy. θ is the angle between the ray and the horizontal. This picture is based on a figure from "Fundamentals of Marine Acoustics" by JERALD W. CARUTHERS [3].

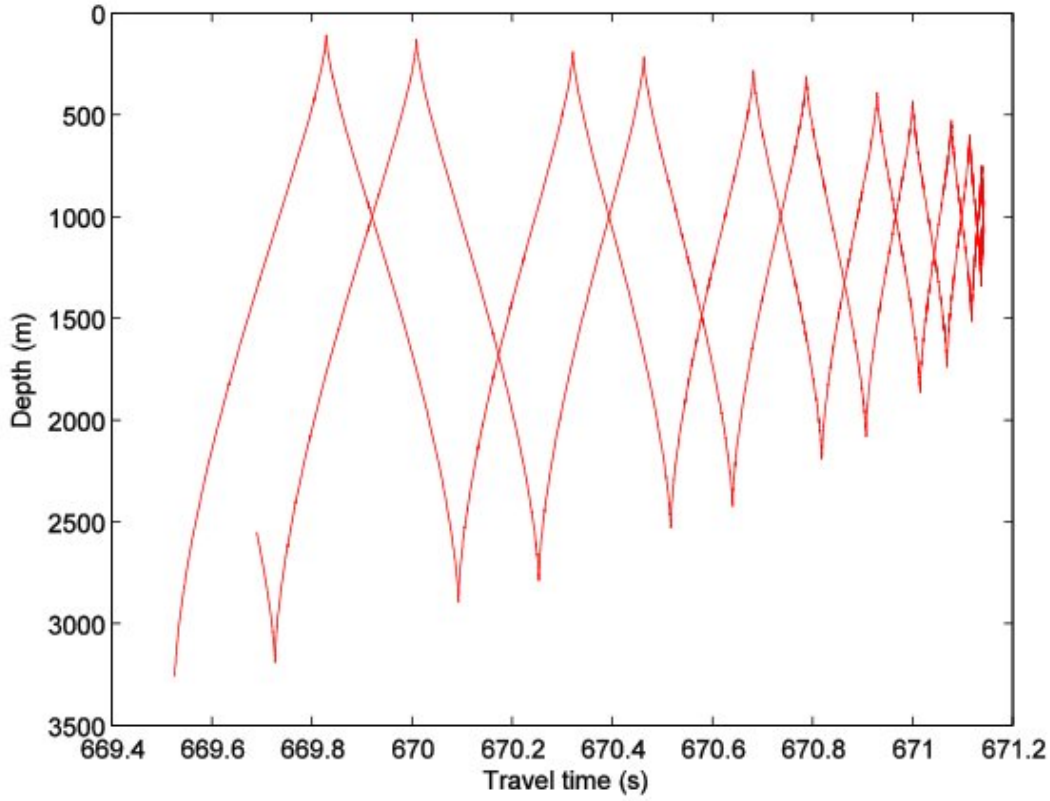

Figure II.2: The figure shows the ray arrivals as a function of depth and travel time. This plot is a 1000 km propagation of rays with the source at a depth of 1000 m. A canonical sound speed profile is used.

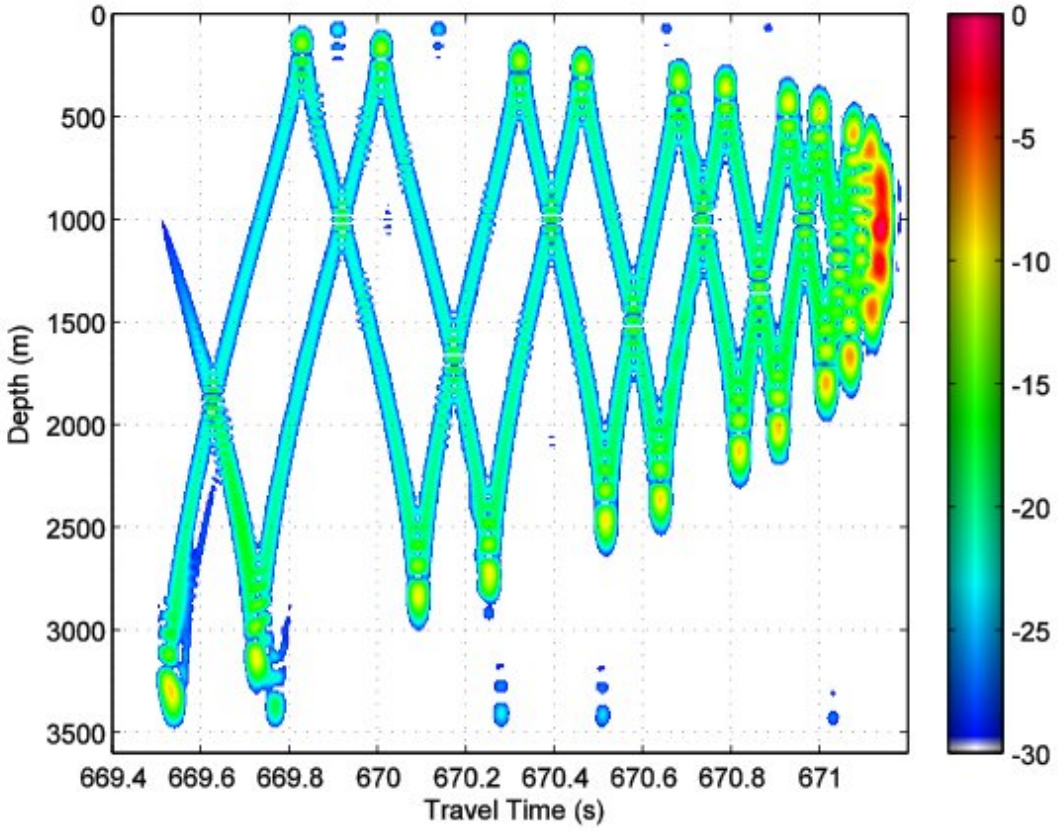

Figure II.3: This figure shows a broadband PE simulation. The wavefront is obtained by using a PE approximation. A canonical sound speed profile is used. The source is at 1000 m depth. Wavefronts are received at 1000 km range. The color bar shows the sound intensity up to 30 dB below the peak intensity. A center frequency of 100 Hz and a bandwidth of 25 Hz are used. The total number of frequencies is 201.

Chapter III

MODELING OF BOTTOM INTERACTING SOUND

III.1 Introduction

Interaction of sound with the bottom is significant in many ocean acoustic experiments, especially in shallow-water cases. Bottom interaction strongly affects sound propagation in short-range shallow-water experiments. In some cases, even long-range sound propagation can be affected by bottom interaction. Bottom interaction could change the intensity of the sound depending on the nature of the bottom. Bottom loss could include both refracted sound and shear contributions. So it is important to be able to model the bottom-interacting sound. Broadband simulations of bottom-interacting sound using the actual elastic bottom parameters is a challenging task and may not be feasible in some cases (see for example, BASSEX in Chapter V). Using a complex-density (CD) equivalent fluid in such cases has important advantages.

As an example, a serious problem raised in a tomography experiment called the North Pacific Acoustic Laboratory (NPAL) experiment was the mismatch of the travel times of the arrival signal in the experiment with that of the model. A 75 Hz broadband acoustic source near Kauai was used in the experiment. The source was located at a depth of 810.90 m. The signals were recorded on an array of receivers near California at a range of 3890 km, and in the Gulf of Alaska at a range of 3336 km. Since the source is bottom mounted and the seafloor near the source is very steep, sound interaction with the bottom complicated the numerical simulations. Simulations with sound reflections from steep bottoms, highly range-dependent bathymetry and a bottom with volcanic origins (which supports high shear wave speeds) is a severe challenge to ocean acoustic simulations. Bottom interaction of the sound must be taken into account for the simulations in this case. The inability to identify the recorded acoustic arrivals with arrivals in numerical simulations was successfully resolved by using the expanded version of CD equivalent fluid modeling of bottom interacting sound in the simulations [22].

Zhang and Tindle developed a method to mimic a soft solid seafloor by using a complex-density equivalent fluid approximation [21]. An expanded version of this model has been developed recently called the Expanded Equivalent Fluid (EEF) method [22, 32]. The details of these methods are discussed in this chapter.

III.1.1 The Seafloor

The bottom of the ocean is called the seabed or seafloor. According to geophysicists and geologists, the formation of the seafloor is due to seafloor spreading (formation of oceanic crust through volcanic activity and its spreading), continental drift, and global tectonics [11]. The seabed begins at the water-sediment interface. The sound velocity increases with depth in sediments. Because of the weight of the overlying sediments, the porosity decreases. Also, the temperature increases with depth in the seafloor. This is due to the flow of heat from the mantle, through the seabed, and into the water.

Sediments on the seafloor are formed due to a variety of sources, including volcanoes and erosion from land transported into the ocean due to wind and rivers. There are different types of sediments. Some samples are mud, muddy sand, sand, and clay. The sea bottom is represented by bottom parameters. They include density ρ, porosity n, compressional wave velocity c_p, shear wave velocity c_s, and attenuation coefficients of compressional and shear waves (α_p and α_s, respectively). Sound waves in the seafloor are compressional waves. The laboratory values of the porosity n, density ρ, and compressional velocity c_p for different types of sediments and environments are given by Hamilton [1]. These measurements are for 23°C and at 1 atm. The velocity of shear wave c_s and shear modulus G values for different sediments are calculated based on Gassmann's theory [11] since the laboratory measurements of these values are unreliable (the coring process changes the sediment structure). The values of the measured and calculated bottom parameters are given in Table III.1 [11]. n is porosity (percent),

Table III.1: AVERAGE MEASURED AND COMPUTED ELASTIC CONSTANTS, NORTH PACIFIC SEDIMENTS. [from "The elastic properties of marine sediments" by E. L. Hamilton][1]

Sediment Type	Measured			Computed	
	n	ρ	c	G	c_s
Continental terrace (shelf and slope)					
Sand					
Coarse	38.6	2.03	1836	0.1289	250
Fine	43.9	1.98	1742	0.3212	382
Very fine	47.4	1.91	1711	0.5035	503
Silty sand	52.8	1.83	1677	0.3926	457
Sandy silt	68.3	1.56	1552	0.2809	379
Sand-silt-clay	67.5	1.58	1578	0.2731	409
Clayey silt	75.0	1.43	1535	0.1427	364
Silty clay	76.0	1.42	1519	0.1323	287
Abyssal plain (turbidite)					
Clayey silt	78.6	1.38	1535	0.1435	312
Silty clay	85.8	1.24	1521	0.0773	240
Clay	85.8	1.26	1505	0.0483	196
Abyssal hill (pelagic)					
Clayey silt	75.0	1.43	1535	0.1427	364
Silty clay	76.0	1.42	1519	0.1323	287
Clay	77.5	1.42	1491	0.0544	195

ρ is density (g/cm^3;kg/m$^3 \times 10^{-3}$), c is compressional wave (sound) velocity (m/s), G is rigidity (shear) modulus, and c_s is shear wave velocity (m/s).

III.1.2 Equivalent Fluids

Shear in the sea bottom can impact sound propagation. Combined elastic-acoustic methods have been developed previously to model sound propagation, which is affected by shear in the sea bottom. But these methods can have numerical difficulties. These methods (RAMS, OASES (see section II.3 in Chapter II)) are computationally slow and can be unstable for steep bottoms [22]. It is especially difficult to handle shear for a broadband long range propagation using RAMS and OASES.

To see the effects of bottom interactions on sound waves numerically, the reflection coefficient for a soft solid seabed could be well approximated by replacing the ocean bottom with a fluid of suitably chosen parameters. This fluid is known as an equivalent fluid [21]. The advantage of the equivalent fluids is largely computational.

It is found that the use of a complex density (CD) gives an equivalent fluid that approximately reproduces the reflection coefficient of a typical soft solid seabed. The equivalent fluid approximations are very efficient in providing a good approximation to the reflection coefficient of a solid seabed with relatively higher shear wave speeds. Equivalent fluid methods do not work in cases where interface waves or the acoustic propagation in the bottom media are significant [22].

Zhang and Tindle (ZT) have developed a technique to model the soft sea bottoms with low shear speeds. The ZT method involves constructing an effective complex density that mimics the loss due to shear without actually simulating shear wave modes. This method has been expanded to treat all bottom parameters (sound speed in the bottom c_p, shear speed c_s, and density ρ) as free in a curve fit to an elastic reflection coefficient over a specified interval of grazing angle. The technique is referred to as the Expanded Equivalent Fluid (EEF) method.

III.2 The Zhang and Tindle Method

The reflection coefficient of a soft solid seabed with a low shear speed can be well approximated by replacing the seafloor with an equivalent fluid of suitably chosen parameters. This is called an equivalent fluid approximation [21]. Using this method, an equivalent fluid can be obtained for the given values of density of the sea bottom ρ, speed of sound in the bottom c_p, shear speed c_s, frequency f and attenuation coefficients α_p and α_s.

Consider a homogeneous fluid of density ρ_1 and sound speed c_1 lying over a homogeneous solid of density ρ_2, compressional wave speed c_2 ($c_2 > c_1$), and shear wave speed c_s ($c_s < c_1$). α_p and α_s are the attenuation coefficients of compressional and shear waves respectively. α_p

and α_s units are dB$/\lambda$.

The reflection coefficient for plane waves in medium 1 incident on the fluid-solid interface can be written as,

$$V_{fs}(k) = \frac{\gamma_1[\frac{\rho_2 P(k)}{\rho_1}] - i\eta_2}{\gamma_1[\frac{\rho_2 P(k)}{\rho_1}] + i\eta_2} \tag{III.1}$$

$$k = \frac{\omega}{c_1} cos\theta_z \tag{III.2}$$

where k is the horizontal wave number, θ_z is the grazing angle (it is the angle between the incident sound ray and the interface), and ω is the angular frequency.

The parameter $P(k)$ in equation III.1 is expressed as,

$$P(k) = \left(1 - \frac{2k^2}{[\frac{\omega}{c_s} + i\alpha_s]^2}\right)^2 + \left(\frac{i4\eta_2\gamma_s k^2}{[\frac{\omega}{c_s} + i\alpha_s]^4}\right)$$

In the absence of shear wave propagation $P(k)$ is 1. In the ZT method, ρ_2' is the effective complex density for the equivalent fluid. It is set as $\rho_2' = \rho_2 P(k)$ and taking the limit as $k = \frac{\omega}{c}$ (by setting $\theta_z = 0^\circ$), The expression for ρ_2' is written as

$$\rho_2' = \rho_2 \left[\left(1 - \frac{2}{(\frac{c_1}{c_s} + \frac{i\alpha_s c_1}{\omega})^2}\right)^2 + \frac{i4[1 - (\frac{c_1}{c_2} + \frac{i\alpha_2 c_1}{\omega})^2]^{\frac{1}{2}}[(\frac{c_1}{c_s} + \frac{i\alpha_s c_1}{\omega})^2 - 1]^{\frac{1}{2}}}{(\frac{c_1}{c_s} + \frac{i\alpha_s c_1}{\omega})^4}\right] \tag{III.3}$$

At low grazing angles, the ZT method performs very well in approximating a soft solid seafloor. Energy propagating at low grazing angles dominates the far field. The ZT method does not alter sound speed in the bottom c_p. This method is intended for cases where loss is dominated by sound transmitted into bottom [21].

III.3 The Expanded Equivalent Fluid (EEF) Method

This method is intended for seafloors with higher shear speeds and larger grazing angle intervals or just larger values of grazing angle [22]. This method takes the grazing angle interval, the density of the bottom ρ, sound speed in the bottom c_p, shear speed c_s, and frequency as input and gives an effective complex- density (with real and imaginary parts ρ_r', ρ_i') and effective sound speed in the bottom c_p' as output.

Through a curve fit, a reflection coefficient that best matches with the reflection coefficient of an elastic sea floor can be found. The EEF method gives the effective complex-density, $\rho' = \rho'_r + i\rho'_i$, and an effective sound speed in the bottom, c'_p, for the reflection coefficient that is obtained in the matching process.

A cost function is used to find a complex-density whose reflection coefficient has the minimum difference from the reflection coefficient of a given elastic bottom. In order to compare the reflection coefficient of an equivalent fluid to the reflection coefficient of an elastic solid, the cost function C_v can be written as

$$C_v = \frac{1}{N_i}\Sigma_{\theta_i}\frac{|V_{es}(\theta_i) - V_{ef}(\theta_i)|}{|V_{es}(\theta_i)|} \tag{III.4}$$

where V_{es} and V_{ef} are the reflection coefficients of (see Equation II.6 in Chapter II) an elastic solid and equivalent fluid respectively. θ_i is a set of integer values of the angles, and N_i is the total number of those angles.

There have been preliminary investigations of the limitations of the EEF approximation. The limitations of this method are understood by comparing a known elastic seafloor to some CD equivalent fluids. The original expanded equivalent fluid and two new versions of the CD equivalent fluid called metric 1 and metric 2 are used to compare with an elastic bottom. A metric is a cost function which can be expressed as shown in the Equation III.4. The original metric (C_{orig}) and the new metrics C_{M1} and C_{M2} are expressed as

$$C_{orig} = \frac{1}{N_i}\Sigma_{\theta_i}\frac{|V_{es}(\theta_i) - V_{ef}(\theta_i)|}{|V_{es}(\theta_i)|} \tag{III.5}$$

$$C_{M1} = \frac{1}{N_i}\Sigma_{\theta_i}\frac{||V_{es}(\theta_i)| - |V_{ef}(\theta_i)||}{|V_{es}(\theta_i)|} \tag{III.6}$$

$$C_{M2} = \frac{1}{N_i}\Sigma_{\theta_i}\frac{||V_{es}(\theta_i)|^2 - |V_{ef}(\theta_i)|^2|}{|V_{es}(\theta_i)|^2} \tag{III.7}$$

The original EEF (C_{orig}) is a phase sensitive version. The two metrics (C_{M1} and C_{M2}) are magnitude-based versions since they consider only magnitude of the reflection coefficient (which is a complex number). C_{M1} and C_{M2} do not consider phase effects [33]. These versions are compared using bottom loss vs. grazing angle plots, and single frequency transmission loss vs. range plots for a soft bottom case (density $\rho = 1700$ kg/m^3, sound speed in the bottom $c_p = 1700$ m/s, and shear speed $c_s = 600$ m/s). Figure III.1 shows the bottom loss vs. grazing angle for the elastic bottom, the original EEF, the Zhang and Tindle, and the metric 1, 2. The bottom loss curve from the original EEF equivalent fluid should capture the reflection

characteristics of the elastic bottom mainly between grazing angle interval 10.5° to 30.2° (since the original EEF equivalent fluid was obtained using this angular interval). Even the magnitude-based versions (metric 1 and 2) roughly captured the bottom characteristics to some extent.

The transmission loss curve from the phase sensitive version (the original EEF) matches well with the OASES TL curve compared to the TL from the Zhang and Tindle method. A no shear case was also included for comparison purposes (see Figure III.2). An acoustic source depth of 7 m, a flat bottom depth at 650 m was used in the simulation. Transmission loss was shown for up to 12 km range. The same environment conditions were used to obtain Figure III.3. The TL curves from the OASES, the original EEF and the magnitude-based versions (metric 1 and metric 2) is depicted in III.3. From the plot, it is clear that magnitude-based versions could not yield the correct acoustic result (based on the comparison with OASES).

III.3.1 Ray Analysis to Find a Suitable Grazing Angle Interval

Ray analysis has been used to find a suitable window of grazing angles for different cases. The following are the steps in the process of analysis.

1) A simulation environment can be created using the sound speed profile, bathymetry, source depth, and range parameters.

2) A ray simulation can be performed using this environment. The maximum number of bottom bounces and launching angle interval are imposed. The simulation provides information on the number of rays that are surface or bottom reflected or both surface and bottom reflected and also their relevant grazing angles. A ray histogram with the number of reflections as a function of grazing angle θ_z can be obtained based on the simulation results.

The ray histogram obtained from the ray analysis is used to understand the grazing angle interval that is relevant to a specific experiment. An example of a ray histogram is given in Figure III.4. This histogram is obtained for the Basin Acoustic Seamount Scattering EXperiment (BASSEX, see Chapter V) case. From the figure, it is found that the grazing angle interval 25° to 65° is important in this case. A total of 2801 rays with launch angles from $-70°$ to $+70°$ were simulated. Rays which are bounced greater than 4 times from the seafloor are neglected. The angular interval from 25° to 65° is used in the EEF method to find the effective complex-density and the effective sound speed in the bottom for a given elastic bottom.

III.4 Results and Discussion

Elastic shear can have a significant impact on sound propagation when the sound energy interacts with the sea bottom. The Zhang and Tindle equivalent fluid method is not intended for high grazing angles [21]. The expanded equivalent fluid (EEF) method is a numerical technique used to approximately model an elastic sea bottom. In this technique, the complex-density and the effective sound speed in the bottom that best mimic the elastic reflection coefficient are obtained for a set of given parameters including the grazing angle interval, density ρ, sound speed in the bottom c_p, shear speed c_s and acoustic frequency f_c [22]. The EEF method allows flexibility in choosing a grazing angle range.

The results depicted in Figures III.5 and III.6 were generated in acoustic simulations at 100 Hz. The grazing angle range used in these cases is 1° to 20°. In both cases, the source depth is $z_s = 500$ m, the bottom depth is a constant $z_b = 1500$ m, and the sound speed in the water is $c_w = 1500$ m/s. Figure III.5 is obtained using a shear speed of 600 m/s. The other parameters used for the simulation are $\rho = 1700$ kg/m^3, compressional sound speed $c_p = 1700$ m/s, and acoustic frequency $f_c = 100$ Hz. For a range of 100 km, the EEF method clearly shows a reasonable agreement with RAMS and OASES along with the Zhang and Tindle method for the grazing angle interval and acoustic frequency of interest. In this case, the relevant grazing angle values are small. So the ZT approximation is in good agreement with the benchmark cases.

Figure III.6 depicts a hard bottom case in which the EEF method transmission loss (TL) curve clearly agrees with the two bench mark cases OASES and RAMS along with the Zhang and Tindle method. In this case, the bottom parameters are shear speed $c_s = 1100$ m/s, sound speed in the bottom $c_p = 2200$ m/s, density $\rho = 2100$ kg/m^3 and center frequency $f_c = 100$ Hz. From Figure III.6, it is evident that the EEF method can be successfully used to model the sea bottom for a shear speed of $c_s = 1100$ m/s. The ZT method also works well in this environment because of the low grazing angles.

Ray simulations have shown that the grazing angles from 1° to 20° are most important in this geometry. So in this case an equivalent fluid is generated using the EEF method considering the angle range 1° to 20°. For this range, the bottom loss curve using the EEF method is in agreement with the elastic reflection coefficient bottom loss curve for shear speeds 600 m/s and 1100 m/s (See Figures III.7 and III.8).

A comparison between the TL curves for a hard bottom case is shown in Figure III.9. These simulations use bathymetry from the North Pacific Acoustic Laboratory (NPAL) experiment

which is shown in Figure III.10. The experiment took place near Kauai, Hawaii. The source is bottom-mounted at 810.90 m below the sea surface. In this case, the TL curves from the EEF and the Zhang and Tindle method are compared with the TL curve obtained using RAMS [22]. The parameters used are center frequency $f_c = 75$ Hz, density $\rho = 2100$ kg/m^3, compressional sound speed $c_p = 2200$ m/s, and shear speed $c_s = 1100$ m/s. This is indeed a challenging environment for an equivalent fluid acoustic simulation. The TL curve using the EEF method is a better approximation to the NPAL RAMS result than the TL curve using the Zhang and Tindle method.

Figure III.11 shows the effect of a much harder sea bottom compared to the bottom used for Figure III.10 [22]. The bottom parameters are considered from a Collins example of a hard bottom [34]. In this case, the source depth $z_s = 25$ m, the bathymetry is a constant $z_b = 600$ m, sound speed in the water $c_w = 1500$ m/s, acoustic frequency $f_c = 20$ Hz, density $\rho = 2000$ kg/m^3, sound speed in the bottom $c_p = 3400$ m/s, and shear speed $c_s = 1700$ m/s were used. The relevant grazing angle interval used in the EEF method for this case was $1 - 30^\circ$. For these extreme bottom parameters and wide angle range due to shallow water, the modeling is more difficult for both the EEF and the ZT methods. The EEF method offers a more effective representation of the bottom compared to the ZT method as shown by the TL curve. But still, the expanded method does not provide an effective model for the extreme parameters of this elastic material.

Data from BASSEX have been examined to generate estimates of elastic properties of the seafloor near Kauai, Hawaii. Figure III.12 is produced for the bottom parameters $\rho = 2100$ kg/m^3, $c_p = 2200$ m/s, and $c_s = 1100$ m/s. Figure III.12 consists of RAMS, EEF, and Zhang and Tindle transmission loss curves for a range of 3.59 km. This is a good example of short range and shallow water simulation. A suitable set of grazing angles for the EEF method are obtained from the ray analysis. These grazing angles are used to calculate the bottom parameters. In this case, the grazing angle interval 25° to 65° is used to get the effective complex-density bottom parameters. This grazing angle window is obtained from the ray histogram (Figure III.4). The acoustic source is the same as NPAL with $f_c = 75$ Hz. Big angular intervals are relevant in this case since it is a short range, shallow water experiment. Using the EEF method is the best choice in this case since the big grazing angular intervals are relevant. It is evident from Figure III.12 that the TL curve from the EEF method is in better agreement with RAMS than the Zhang and Tindle TL curve.

Discrepancies remain at intermediate ranges. However, the acoustic field at those shorter ranges is impacted by a slightly different interval of grazing angle than the final range of 3.59

km where accuracy is most desired. From Figures III.5, III.6, III.9, and III.12, it is clear that the EEF method can be used to approximate an elastic seafloor and offers improvements over the Zhang and Tindle method when higher grazing angles are relevant.

Figure III.13 shows another instance of the capability of the EEF method. The environment used in this example is considered from a previous airgun ocean acoustic experiment [4] except for the ocean bottom. The bottom used in this case is flat at 650 m depth for simplification. The reason for using the flat bottom is that, in the benchmark method OASES, simulations for range dependent bottoms are complicated. The acoustic source depth is 7 m. The receiver range is 12 km from the source. This simulation was run for a single frequency of 100 Hz. The elastic bottom parameters used in the simulation are density $\rho = 1700$ kg/m^3, sound speed in the bottom $c_p = 1700$ m/s, and shear speed $c_s = 600$ m/s. This bottom has relatively low shear speed and it can be considered as soft. Figure III.13 shows the comparison of transmission loss curves from the EEF and the ZT method with TL of OASES. The figure clearly shows that the TL from the EEF method is in better agreement with the benchmark OASES TL curve than the ZT TL curve. One of the main reasons that the EEF method outperformed the ZT method in this case is because the EEF method has the flexibility of choosing the relevant grazing angle range for this environment. The relevant grazing angle range obtained from the ray analysis is 10.5°-30.2°. The CD equivalent fluid parameters obtained using this angular interval and the bottom parameters are $\rho' = 902.1 + i137.5$ kg/m^3, and effective sound speed in the bottom $c'_p = 1703.7$ m/s.

Figure III.14 shows a multi-frequency acoustic signal generated using an equivalent fluid selected for a grazing angle window of 25° to 65°. The source depth $z_s = 810.90$ m. The bottom depth increases as the range increases up to 3.59 km [22]. The bathymetry for this simulation is shown in Figure V.1. Figure III.14 is consistent with data indicating a reflected arrival between 3 and 3.4 s, with appropriate relative levels [32]. A broadband source with a center frequency of 75 Hz, a quality factor of 2 was used in the simulation.

III.5 Conclusion

Simulation results obtained using the EEF, the ZT methods, and the standard benchmark methods OASES and RAMS are presented for several different environments. The flexibility and efficiency of the EEF technique has been shown by considering different examples. The EEF method has more free parameters to obtain a suitable CD equivalent fluid that better represents an elastic bottom. Another important advantage of this method is that it can be successfully used

in cases where higher values of grazing angle are relevant. The Zhang and Tindle (ZT) method is effective at low grazing angles (approximately below 20°). This method can be applied to cases with shear speed up to about 1100 m/s. The EEF method is also applicable to the bottoms where shear speeds are as high as 1100 m/s [22]. The main advantage of the EEF method lies in its flexibility in selection of the grazing angle interval. Also, there are more free parameters in this method. For example, in BASSEX case the suitable grazing angle interval range is 25° to 65°. See Figure III.4. Obviously, the ZT method cannot work in the BASSEX environment. Using the EEF method is suitable in this case.

But, for a very challenging environment ($c_s = 1700$ m/s, $c_p = 3400$ m/s, and $\rho = 2000$ kg/m^3) with shear speed higher than the speed of sound in water, both ZT and EEF methods are unsuccessful as shown in Figure III.11. For large grazing angles, the EEF technique fails for some media.

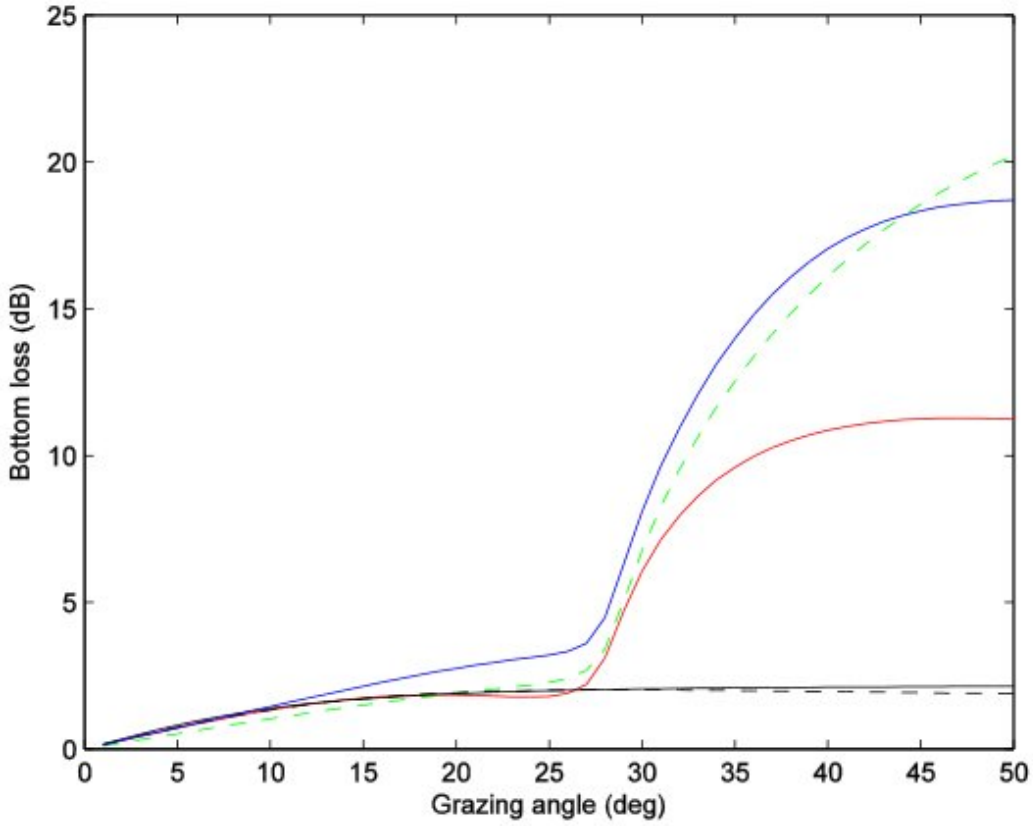

Figure III.1: This figure shows bottom loss vs. grazing angle for a soft elastic bottom (red) compared to the original EEF (green), metric 1 and 2 (black) and the Zhang and Tindle equivalent fluid (blue).The soft bottom is characterized by sound speed in the bottom $c_p = 1700$ m/s, shear speed $c_s = 600$ m/s, and density $\rho = 1700$ kg/m^3.

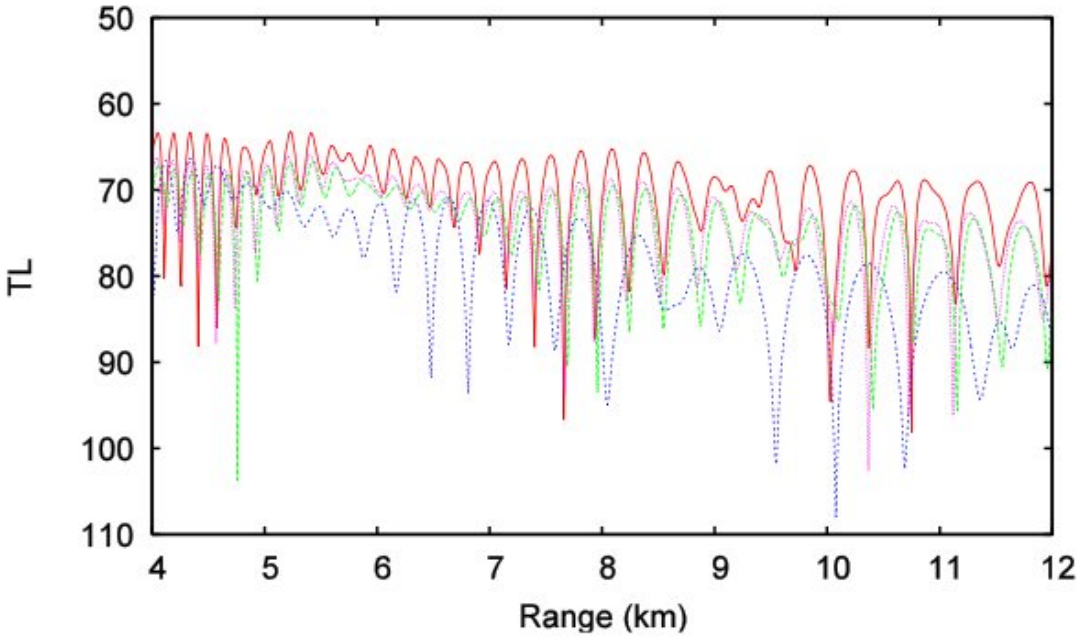

Figure III.2: Transmission loss vs. range plot of the OASES benchmark simulation (magenta) compared to a simulation that neglects shear (red), the original EEF (green), and the Zhang and Tindle equivalent fluid (blue) for a soft bottom case. The frequency chosen for this simulation was 100 Hz. The plot depicts transmission loss from 4 to 12 km.

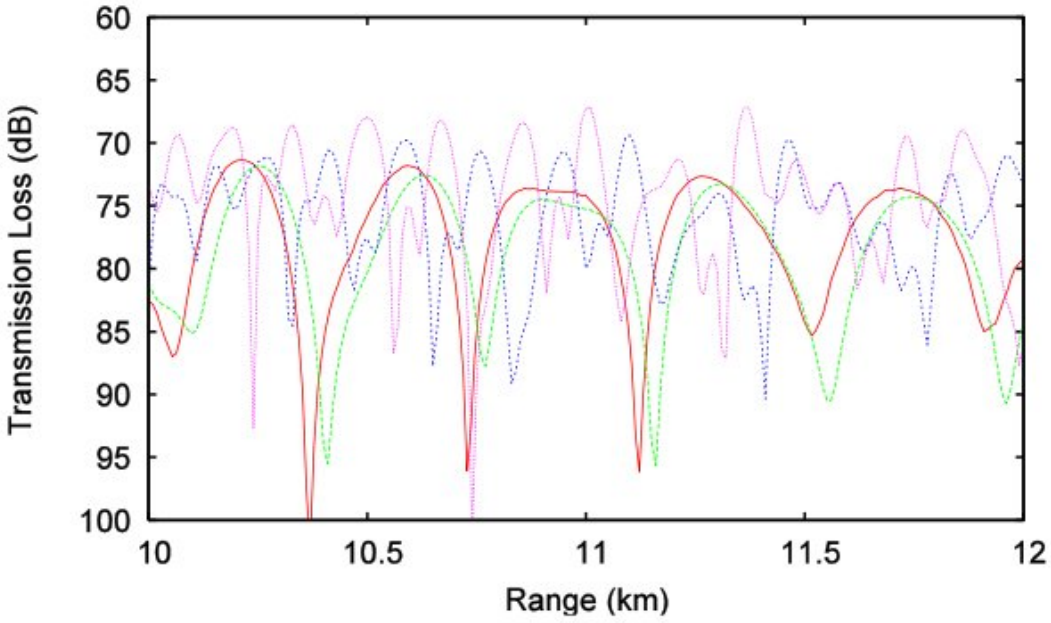

Figure III.3: Transmission loss vs. range plot of the OASES benchmark simulation (red) compared to TL of the original EEF simulation (green), the metric 1 (blue), and the metric 2 (magenta). The frequency chosen for this simulation was 100 Hz. The plot depicts transmission loss from 10 to 12 km.

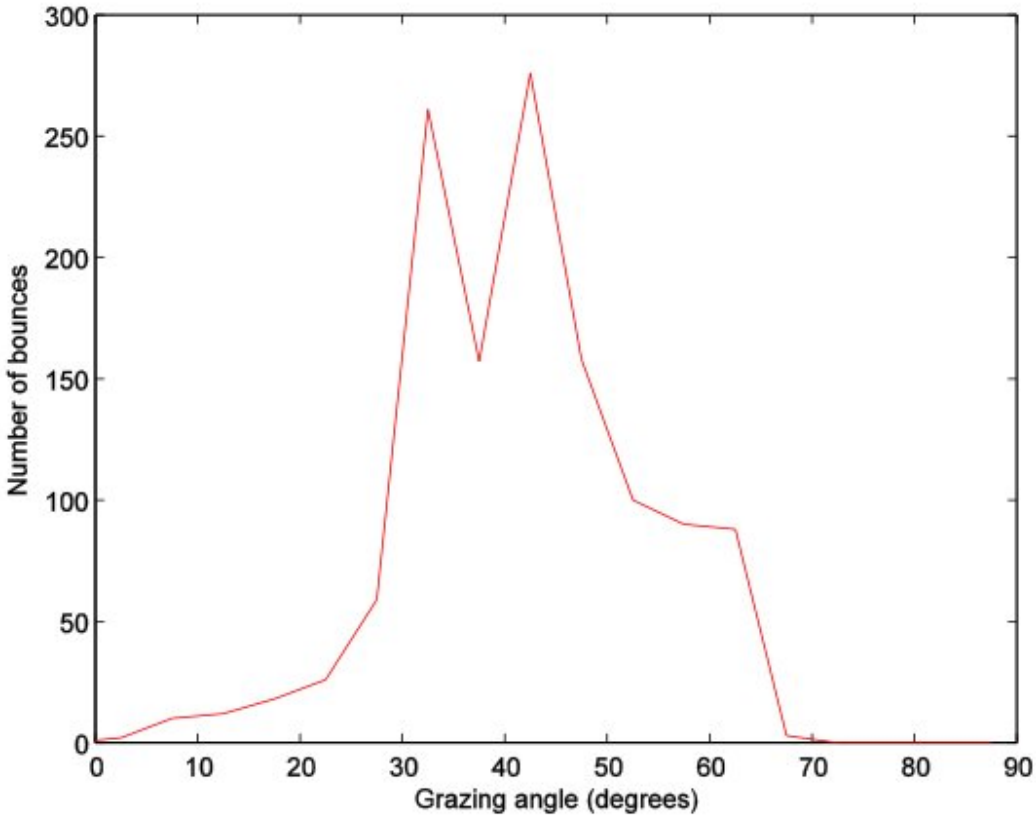

Figure III.4: An example of a ray histogram is shown in the picture. It gives information about the grazing angles that are relevant in the sound propagation for the case of BASSEX. From the figure, the interval of grazing angle from 25° to 65° is most significant.

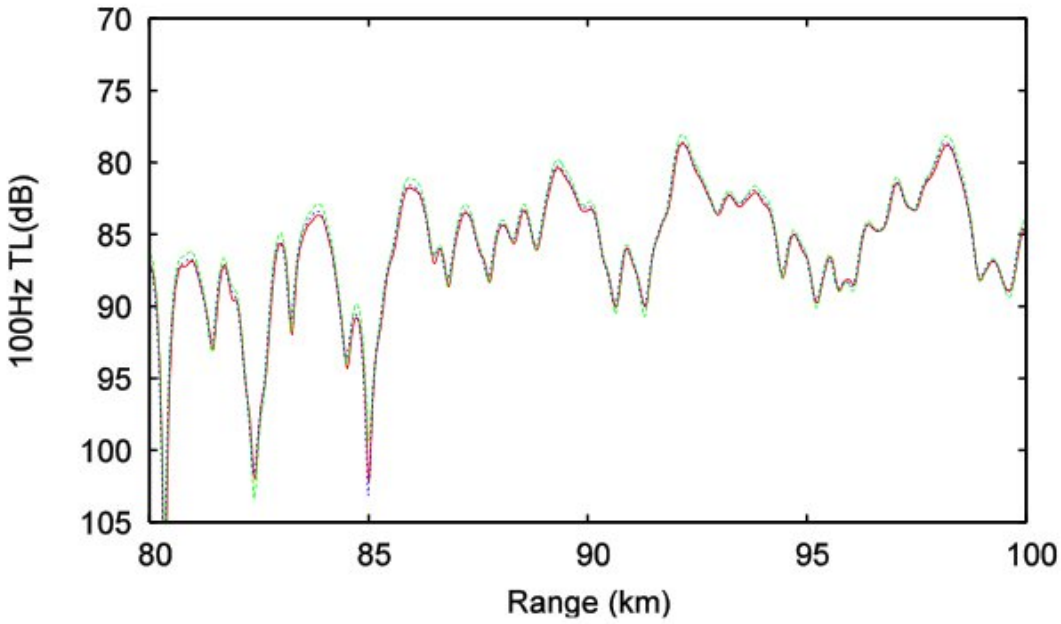

Figure III.5: Transmission loss (TL) curve for a maximum range of 100 km is depicted. It shows the TL curves of RAMS (red line), EEF (green line), and Zhang and Tindle (blue line) for an elastic sea bottom with $\rho = 1700$ kg/m^3, $c_p = 1700$ m/s, and $c_s = 600$ m/s. The acoustic frequency is $f_c = 100$ Hz. The bottom is flat at 1500 m. The grazing angle interval used in this case is 1° to 20°.

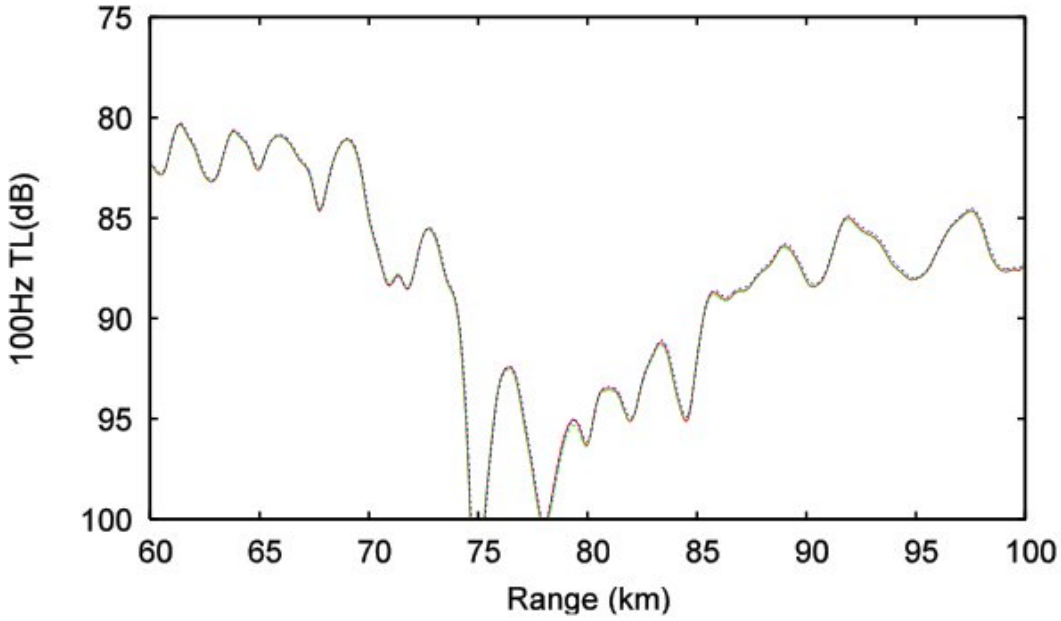

Figure III.6: Transmission loss (TL) versus Range (km) plot for a range of 100 km is shown. It is a comparison between OASES (red curve), EEF (green curve), and Zhang and Tindle (blue curve). The corresponding bottom parameters are $\rho = 2100$ kg/m^3, $c_p = 2200$ m/s, $c_s = 1100$ m/s, and $f_c = 100$ Hz. The bottom is flat at 1500 m. The grazing angle interval used in this case is 1° to 20°.

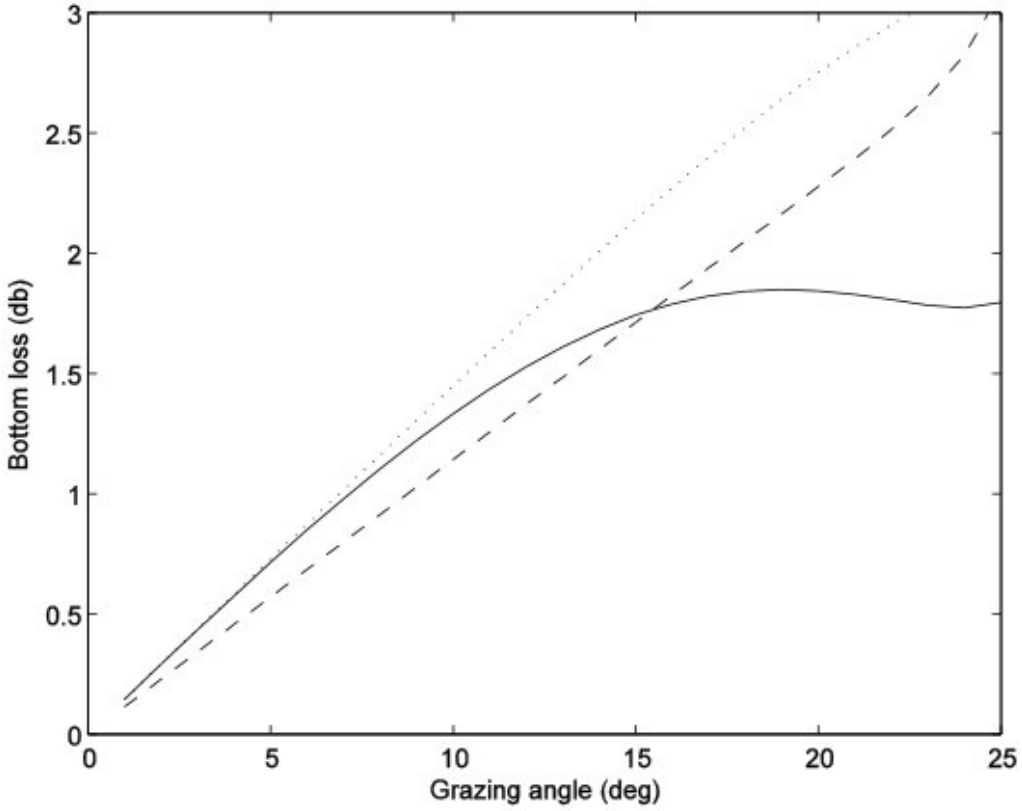

Figure III.7: Bottom loss (dB) as a function of grazing angle (θ_z) for a shear speed of 600 m/s is shown. It shows a comparison between the bottom loss curves from the elastic reflection coefficient (solid line), the Zhang and Tindle method (dotted curve), and the EEF method (dashed curve). The parameters used in this case are $c_p = 1700$ m/s, $\rho = 1700$ kg/m^3, and $c_s = 600$ m/s.

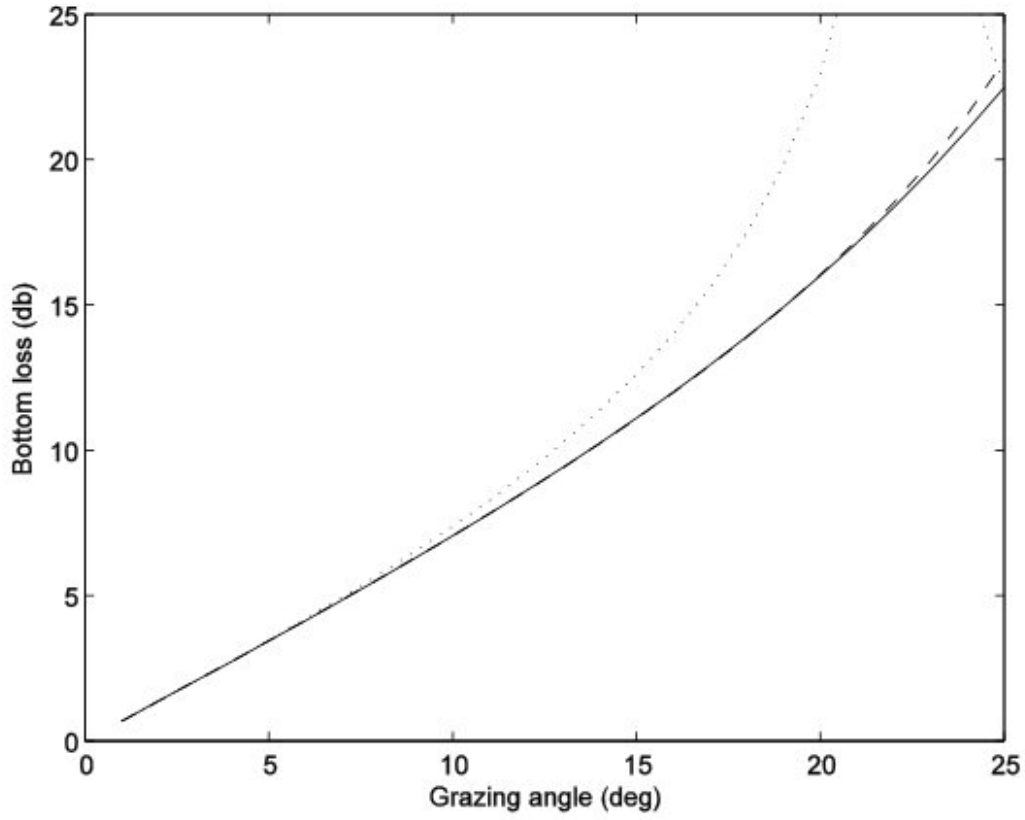

Figure III.8: Bottom loss (dB) as a function of grazing angle (θ_z) for a shear speed of 1100 m/s is depicted. In this case, the EEF result was determined for the grazing angle interval up to 20°. The solid curve is the elastic reflection coefficient, the dashed curve is from the EEF method, and the dotted curve is from the Zhang and Tindle method. The parameters used in this case are $f_c = 100$ Hz, $c_p = 2200$ m/s, $\rho = 2100$ kg/m^3, and $c_s = 1100$ m/s.

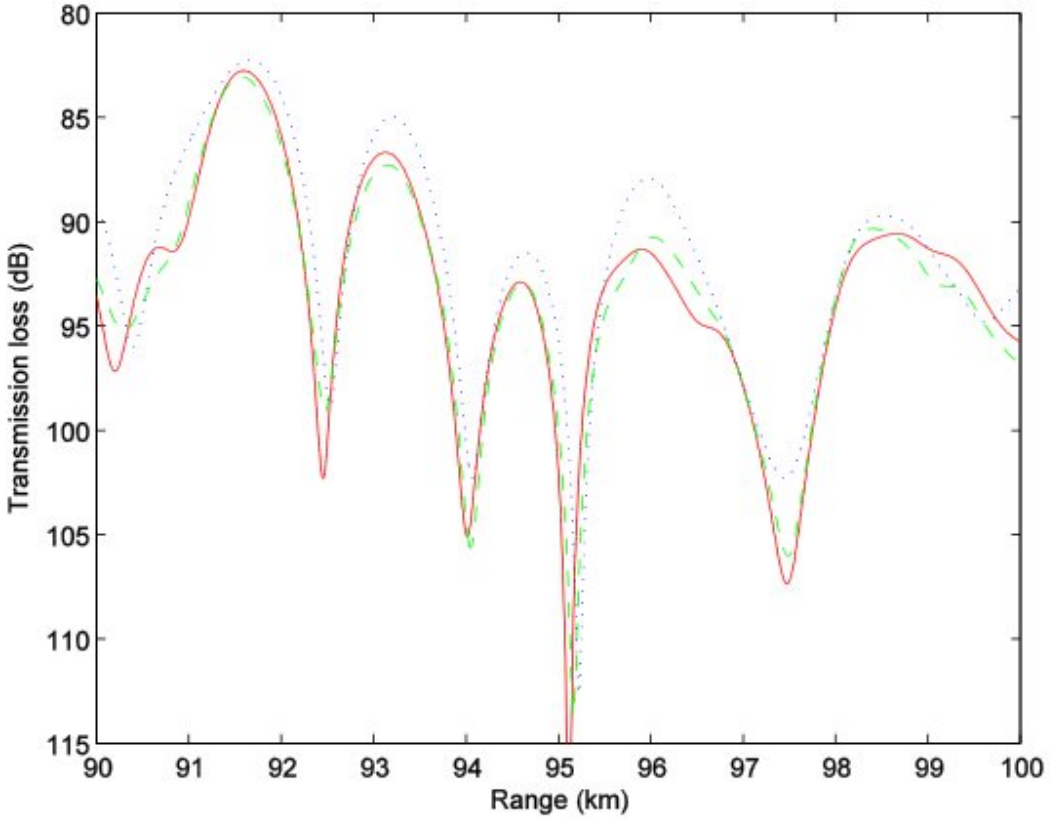

Figure III.9: Transmission loss (dB) as a function of range (km) for an NPAL case is shown. The red curve is from RAMS, the green line is from the EEF method, and the blue line is from the Zhang and Tindle method. The parameters used in the simulation are $f_c = 75$ Hz, $c_s = 1100$ m/s, $c_p = 2200$ m/s, and $\rho = 2100$ kg/m^3.

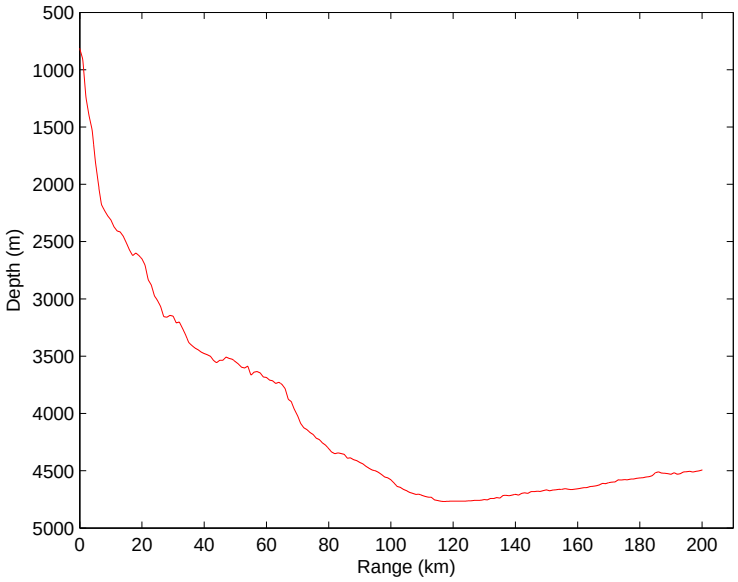

Figure III.10: The near source sea bottom variation as a function of range in the NPAL experiment is shown in the figure. The source is approximately 2 m above the seafloor and the source depth is 810.90 m.

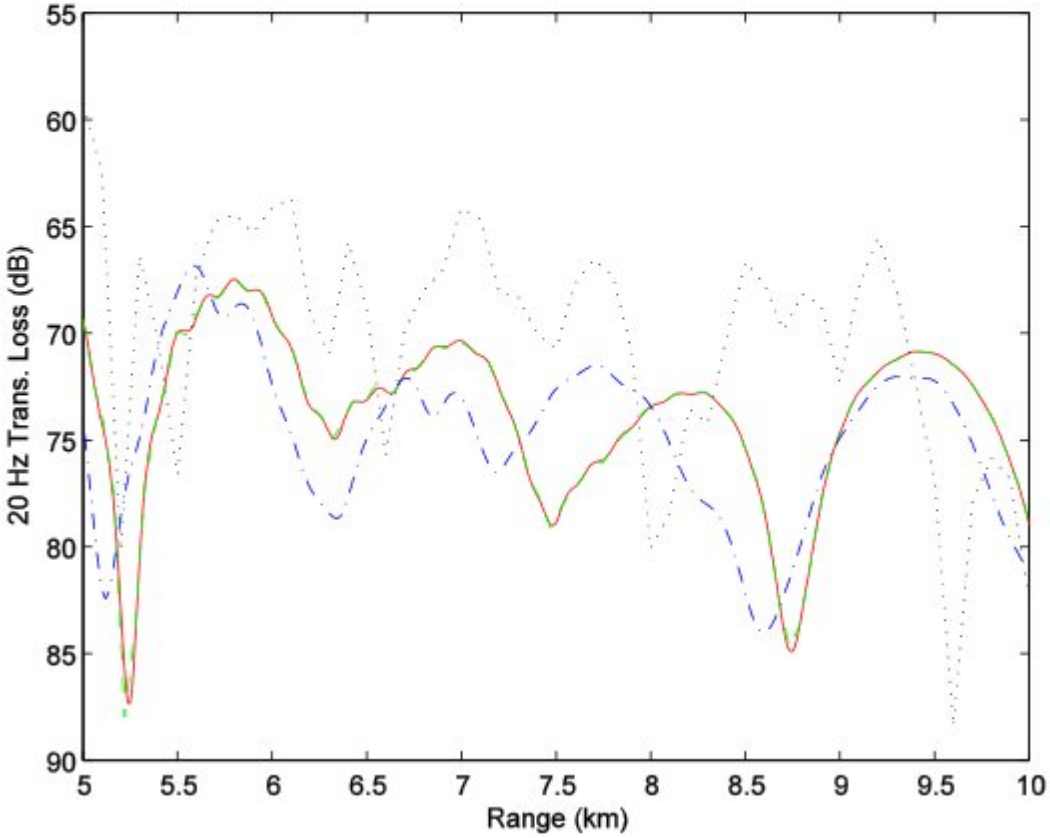

Figure III.11: Transmission loss (dB) as a function of range (km) is shown. The red curve is from a Collins example of a hard bottom using RAMS, the green curve is from OASES, the blue curve is from the EEF method, and the black curve is from the Zhang and Tindle method. The parameters used in the simulation are $f_c = 20$ Hz, $c_s = 1700$ m/s, $c_p = 3400$ m/s, and $\rho = 2000$ kg/m^3.

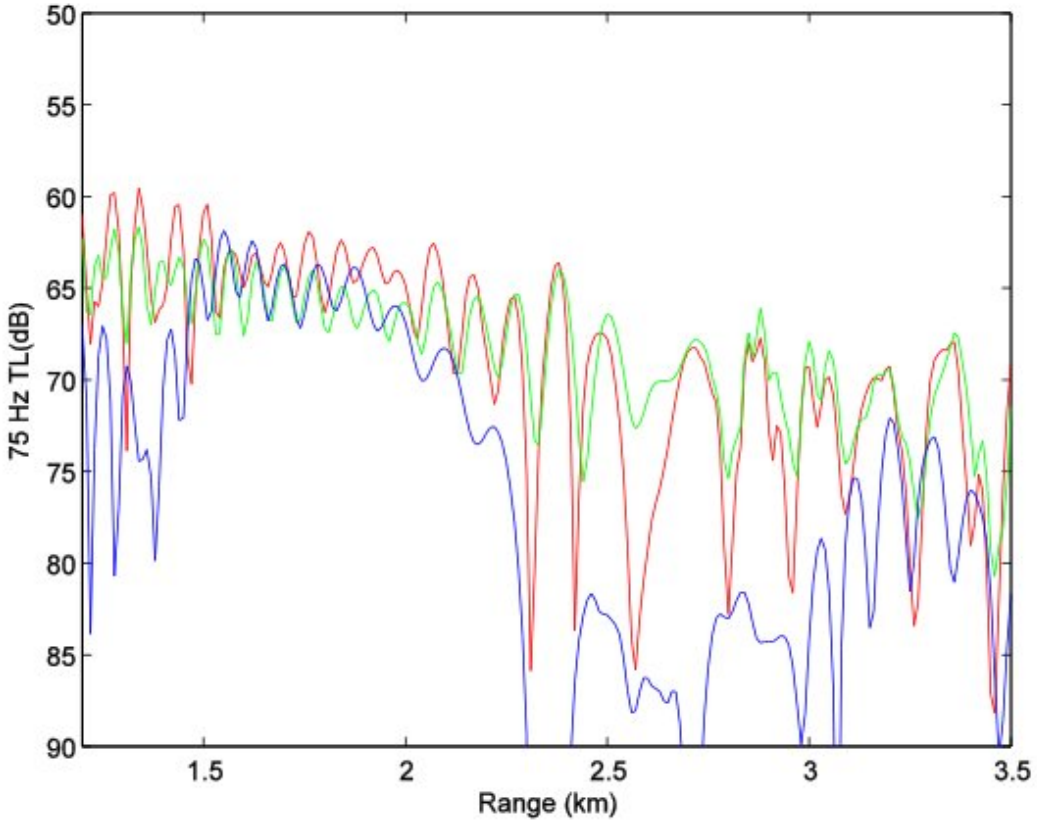

Figure III.12: Transmission loss (dB) as a function of range (km) for the BASSEX case is shown. The red line is from RAMS, the green line is from the EEF method, and the blue line is from the Zhang and Tindle method. The parameters used in the simulation are $f_c = 75$ Hz, $c_s = 1100$ m/s, $c_p = 2200$ m/s, and $\rho = 2100$ kg/m^3. The NPAL bottom was used. The source is at 810.90 m depth.

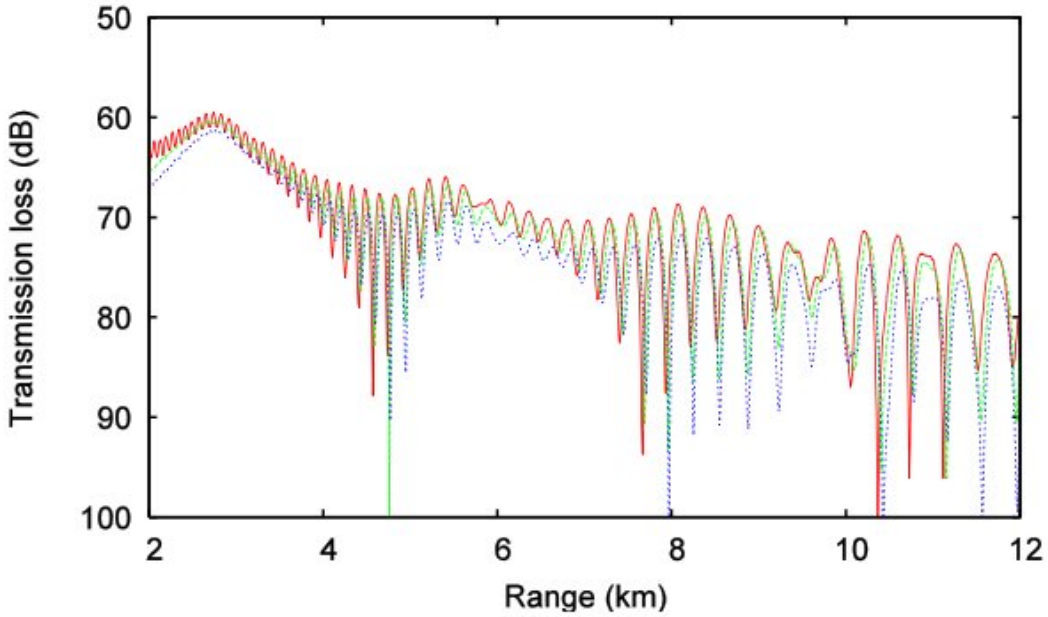

Figure III.13: Comparison of transmission loss (dB) between a benchmark simulation called OASES (red line), the EEF (green line) method, and the Zhang and Tindle method (blue line) is depicted in the figure. The single frequency used in the simulation was 100 Hz. Loss level from the EEF method is in better agreement with OASES. The environment used in this simulation is similar (except the bathymetry) to a previous ocean acoustic airgun experiment [4].

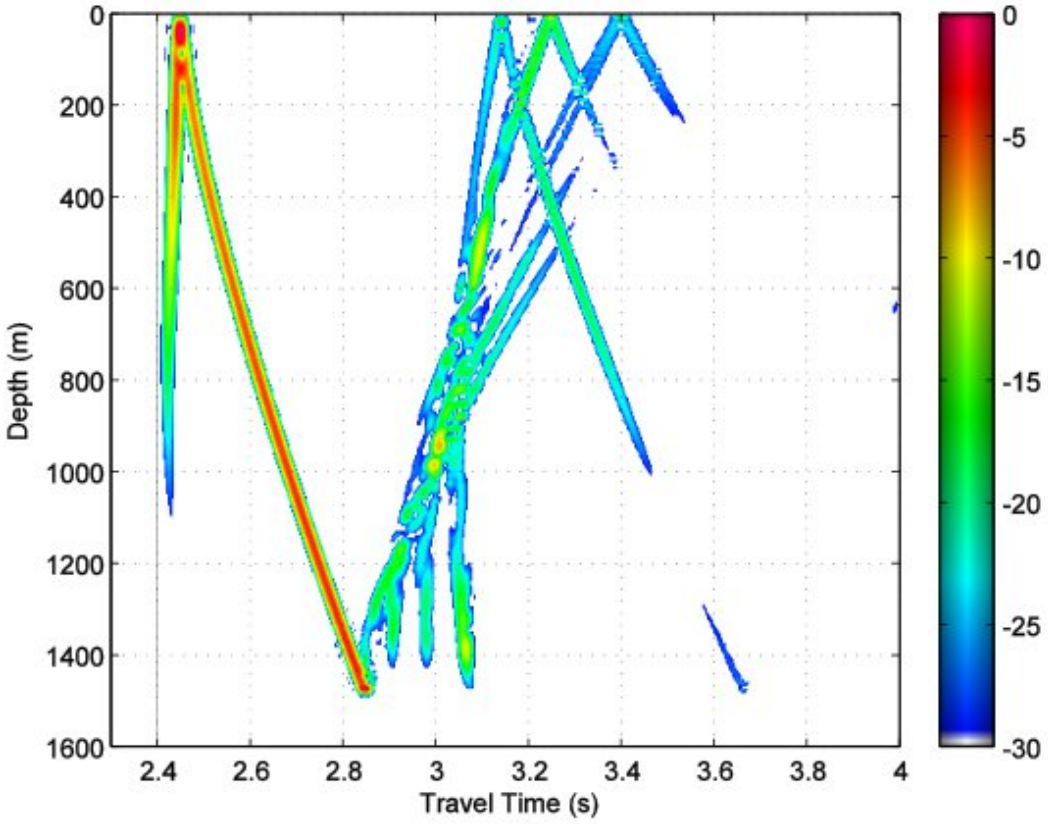

Figure III.14: A broadband time front generated using the EEF method. The acoustic signal is shown as a function of depth and travel time at a range of 3.59 km. The parameters used to obtain the complex densities are $f_c = 75$ Hz, $c_s = 999.5$ m/s, $c_p = 2276.7$ m/s, and $\rho = 2066.8$ kg/m^3.

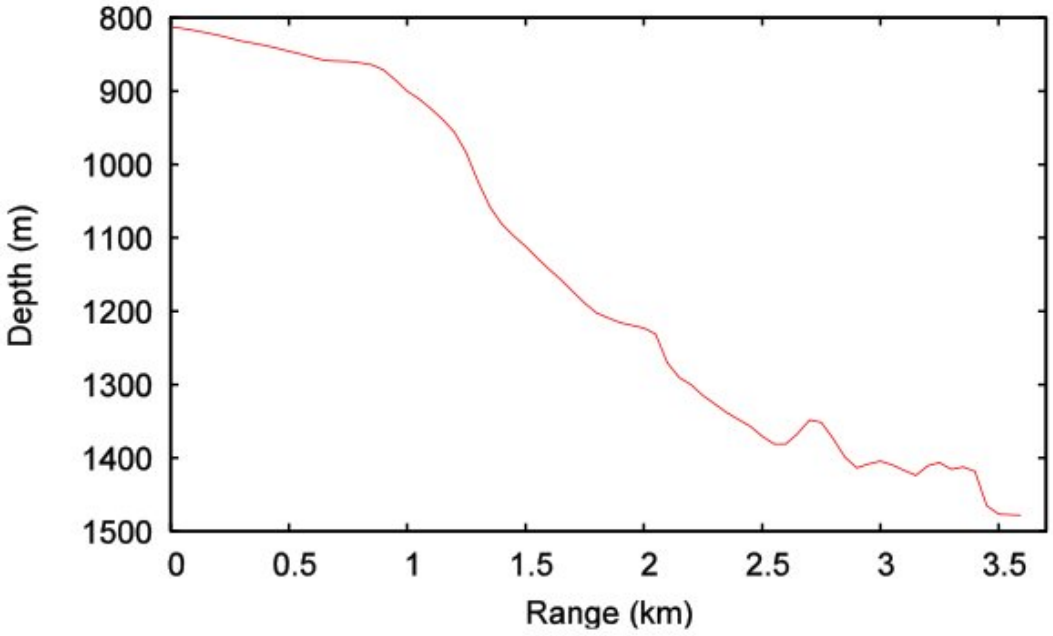

Figure III.15: The bathymetry of BASSEX for a range of 3.59 km is shown in the figure. The bottom is steep for the entire range. The varying bottom made the environment highly range-dependent. The source is at 810.90 m depth [5].

Chapter IV

AIR GUN SOURCES

IV.1 Airguns and Concerns About Marine Mammals

The purpose of seismic surveys is often to locate and estimate the size of oil and gas reserves beneath the ocean floor. These surveys are active in many areas around the world. Airguns have been used in these surveys for many years. An example of a ship using this method for oil exploration is shown in Figure IV.1. An airgun array consists of multiple airguns. The survey ship in the figure has an array of airguns towed behind it [6].

Airguns are mechanical devices which can produce controlled seismic energy. These are advanced seismic sources that are being extensively used by the petroleum industry for exploration. An airgun is a stainless steel cylinder filled with high-pressure air. When an airgun is fired, a large amount of seismic energy is released almost instantaneously into the surrounding water column creating a loud signal. The amplitude or loudness of an airgun depends on volume and pressure of the air inside the airgun cylinder and the airgun's depth in the water [7]. The generated sound wave can travel through a medium like water or a solid seabed. Some of the energy will reflect and then be received by hydrophones for analysis. An airgun array is designed in a particular way so that the energy emits from a source in a very brief time and penetrates well into the earth. The unit of measurement used for pressure by the acoustic community is the micro-Pascal (μPa) where 1 bar$= 10^{11}\mu$Pa $= 220$ dB re 1μPa [7].

Seismic sources can generate single or continuous pulses. The amount of seismic energy released by an airgun or an array of airgun sources is substantial. These are one of the most intense man-made noise sources in the marine environment. Hence, the amount of impact caused by these guns on marine life is an important concern.

An airgun device consists of one or more chambers filled with compressed air at pressures of 2000 pounds per square inch (psi) to 3000 psi. An airgun array generally consists of 12 to 48 individual guns with different sizes [35]. This array is placed below the water surface and towed behind a ship. The guns are usually placed 3 to 10 m below the water surface. An example of an airgun array with 31 guns is shown in Figure IV.2. The array has the combination of single (white) and cluster guns (green) [36]. Table IV.1 shows the position of airguns in the array,

volume of each gun in the array, and distance to individual gun in the array to the receiver. This information was used in the broadband simulations presented in this Chapter. Guns 19 and 20 are exactly 12 km from the receiver. All other individual or cluster guns are more than 12 km distance from the receiver.

Table IV.1: Airgun array geometry and volume of the individual guns

Gun number	Position coordinates			Volume V (cu.in)	Distance from the receiver(m)
	x(m)	y(m)	z(m)		
1	0.00	-10.40	6.00	150	12014.0045
2	0.00	-9.60	6.00	150	12014.0038
3	3.00	-10.40	6.00	60	12011.0045
4	3.00	9.60	6.00	60	12011.0038
5	5.00	-10.00	6.00	20	12009.0042
6	7.00	-10.00	6.00	40	12007.0042
7	9.00	-10.00	6.00	60	12005.0042
8	11.00	-10.40	6.00	100	12003.0045
9	11.00	-9.60	6.00	100	12003.0038
10	14.00	-10.40	6.00	250	12000.0045
11	14.00	-9.60	6.00	250	12000.0038
12	0.00	-0.40	6.00	100	12014.
13	0.00	0.40	6.00	100	12014.
14	3.00	0.00	6.00	90	12011.
15	5.00	0.00	6.00	60	12009.
16	7.00	0.00	6.00	20	12007.
17	9.00	0.00	6.00	40	12005.
18	11.00	0.00	6.00	70	12003.
19	14.00	-0.40	6.00	250	12000.
20	14.00	0.40	6.00	250	12000.
21	0.00	9.60	6.00	150	12014.0038
22	0.00	10.40	6.00	150	12014.0045
23	3.00	9.60	6.00	150	12011.0038
24	3.00	10.40	6.00	150	12011.0045
25	5.00	10.00	6.00	70	12009.0042
26	7.00	10.00	6.00	40	12007.0042
27	9.00	10.00	6.00	20	12005.0042
28	11.00	9.60	6.00	70	12003.0038
29	11.00	10.40	6.00	70	12003.0045
30	14.00	9.60	6.00	250	12000.0038
31	14.00	10.40	6.00	250	12000.0045

An oscillating bubble in the surrounding water is generated when an airgun is first fired. The high pressure inside the bubble makes it expand rapidly. There will be a bubble train following the first bubble. Since the main interest is the primary pulse, the size of the pulses in the bubble train could be reduced by choosing guns with different volumes. The process of selecting gun volumes to minimize sound levels in the bubble train is called tuning the array. The process of adjusting the firing times of different guns to make all guns discharge simultaneously is called synchronizing the guns.

The sound pressure (amplitude) generated by an airgun array is linearly proportional to the number of guns in the array, linearly proportional to the firing pressure of the array, and directly proportional to the cube root of the volume of the array. The sum of the volumes of all airguns in an array is typically equal to $3000 - 8000$ in^3 [35].

The amount of pressure released when an airgun fires underwater is shown by pressure signature. The signature has three main features.

a) **Direct arrival**: This is the sound produced when the airgun port's first opens;

b) **Source ghost**: This is the reflection of the direct arrival from the surface of the water, and it has opposite polarity compared to direct arrival;

c) **Bubble train**: This occurs due to the air bubble expansion-collapse cycle.

An airgun's pressure signature has two parameters. They are the strength (amplitude of the sound) and the bubble period. The bubble period is the time between successive bubble pulses [37].

IV.2 Far-field Simulations of Sound from An Array of Airgun Sources

The objective of this project is to simulate farfield sound from an array of airgun sources. The term far field means that the distance from the airgun array where the acoustic output appears to be arriving from a single point source [7]. However, the simulations presented in this Chapter consider array geometry rather than array as a single point source. Several complexities are added in the simulations. It is a short range (12 km), near surface source (7 m), shallow water varying bottom (see bathymetry in Figure IV.4) environment. Short range in the sense that bottom bounces are present even though the bottom is not very steep. Since the bottom is shallow, the presence of bottom interacting sound complicates the simulations. The EEF method has been used to find the effective complex density and effective compressional speed. These parameters are used in broadband simulations to model sound in the farfield which has shear loss from bottom interaction.

IV.2.1 Basic Set-up of Environment for Simulations

A series of simulations have been performed for airgun-array sources using the expanded equivalent fluid to represent the bottom. Instead of treating the source as a point source, the whole array geometry is considered. So the effect of the range offset of airguns is incorporated in the simulations.

The airgun array as shown in Figure IV.2 was used in the simulations. The airgun array source depth is 7 m below the water surface. Far-field simulations are done for a 12 km range. Only guns 19 and 20 are exactly 12 km from the receiver point in the farfield. All other guns are having slightly higher range values as shown in Figure IV.3. The sea bottom structure is shown in Figure IV.4. The bathymetry, source depth, and SSP are considered from a previous study of an airgun experiment [4]. Sound waves interact with the sea bottom in this environment.

An airgun array signature is a short duration pulse. An airgun array signature shows amplitude variation (dB relative to 1μ Pa/Hz at a range) as a function of frequency (Hz). Airgun array signatures are broadband, since they consist a whole range of frequencies. An airgun array source horizontal signature at 1000 m is considered from a previous study to use in the simulation [7]. The horizontal signature is shown in Figure IV.5. This horizontal amplitude spectrum is used to get final intensity values in the farfield.

Airgun arrays used in the oil industry will be operated so that most of the energy released from the guns in an array is directed downward. Because of this, the vertical signature from an airgun array has an overall higher amplitude compared to the horizontal signature.

Parabolic-equation broadband simulations using equivalent fluids are performed for four different cases. These are

(a) No shear case with a soft bottom,

(b) No shear case with a hard bottom,

(c) Bottom with shear speed of 600 m/s case, and

(d) Bottom with shear speed of 1100 m/s case.

Actual elastic bottom parameters and complex-density equivalent fluid parameters for soft and hard bottoms are shown in Table IV.2. The CD parameters were obtained using the EEF method by giving the relevant grazing angle interval $10.5^\circ - 30.2^\circ$, bottom parameters, and center frequency 427.5 Hz as input. Bottom density ρ units are kg/m^3, sound speed in the bottom c_p and shear speed c_s units are m/s. The EEF method estimates the effect of shear by

Table IV.2: Soft and hard bottom parameters

Bottom type	Elastic bottom parameters	Complex-density equivalent fluid parameters
Soft	ρ=1600 c_p=1700 c_s=600	ρ'_r+ρ'_i=851.9+i128.0 c'_p=1703.8
Hard	ρ=2100 c_p=2200 c_s=1100	ρ'_r+ρ'_i=95.7+i1492.4 c'_p=3000.0

using suitably chosen parameters. In cases of (a) and (b), the shear parameter is simply ignored.

The frequency range considered for the simulations is from 5.1 to 850.5 Hz. Lower frequencies have less amplitude and cause numerical difficulties and have been ignored. The center frequency $f_c = 427.5$ Hz, and a bandwidth= 423 Hz is used. The simulation in each case was done for a total of 4228 frequencies. For this complicated environment involving wide range of frequencies, it is found (from single frequency convergence testing) that the PE broadband simulations involving lower frequencies should be using a higher range step value (dr) and the higher frequencies should be using a lower range step value.

For convergence testing, the environment chosen was similar to the one that is used in PE broadband airgun simulations except for the bottom. A flat ocean bottom at 650 m depth is used in these simulations. The source was at 7 m depth. Transmission loss simulations are performed for a range of 12 km. Transmission loss as a function of range was plotted with different computational grids for comparison purposes. These single frequency simulations are performed for a soft bottom and a bottom that neglects shear. Convergence test results for the no shear case for frequency 20 Hz is shown in Figure IV.6. For the frequency $f = 20$ Hz (a relatively low frequency according to the present simulation environment), computational grids dz= 0.5 m, dr= 5 m (dz is the computational depth step and dr is the computational range step) and dz= 0.5 m, dr= 10 m did not give valid simulation results. Figure IV.6 shows transmission loss curves for three different grids. They are dz= 0.5 m, dr= 25 m (red), and dz= 1 m, dr= 50 m (green), and dz= 0.5 m, dr= 50 m (blue).

For the frequency $f = 600$ Hz (a relatively high frequency according to the present simulation environment), computational grids dz= 0.5 m, dr= 50 m and dz= 1 m, dr= 50 m did not give valid simulation results. Grid parameters dz= 0.5, dr= 5 work well for this high frequency simulations. Based on the transmission loss curves, it is clear that low frequencies must use range step values at least dr= 25 m and high frequencies must use dr= 5 m.

Convergence test results for the soft bottom case for frequencies 20 Hz and 600 Hz are

shown in Figures IV.7 and IV.8 respectively. Benchmark OASES single frequency simulation results for frequencies 20 Hz and 600 Hz were also included in the plots to check for the accuracy. Acoustic results for the soft bottom case have shown that higher frequencies must use a low value of range step.

Based on the convergence test results, in the PE broadband simulations, the frequencies from 5.1 to 44.1 Hz were simulated with a range step $dr = 50$ m for both soft and hard bottom cases. Frequencies from 44.3 to 850.5 Hz were simulated with $dr = 5$ m for soft bottom and $dr = 10$ m was used for hard bottom.

a) **No shear case with a soft bottom**: In this case, the shear in the ocean bottom is ignored. The density of the bottom is 1600 kg/m^3, sound speed in the bottom $c_p = 1700$ m/s, and shear speed $c_s = 0$ m/s. So there is no loss of energy for the sound waves due to shear. However, there is still bottom loss due to compressional waves.
b) **No shear case with a hard bottom**: In this case, the density of the bottom is $\rho = 2100$ kg/m^3, sound speed in the bottom $c_p = 2200$ m/s, and shear speed $c_s = 0$ m/s.
c) **Bottom with shear speed of** 600 **m/s**: This is a relatively small shear speed. Regions of seafloor with shear speeds of about 600 m/s represent an estimate of a higher value that might be found in the Gulf of Mexico.
d) **Bottom with shear speed of** 1100 **m/s**: This is a comparatively higher shear speed. It indicates that the bottom is consolidated. In this case, sound waves which interact with the bottom suffer more energy loss compared to no shear and shear speed of 600 m/s cases.

IV.3 Method

A phase shift method has been used to perform farfield simulations of sound from an array of airgun sources. This method incorporates range deviations as phase shifts.

In the phase shift method, first the complex wave (with real and imaginary parts) values at 12 km range in the farfield are obtained using the broadband PE simulations. These values are considered as reference complex wave values. They are represented with ψ_0. Next, the complex wave values of guns at ranges 12003 m, 12005 m, 12007 m, 12007 m, 12011 m, and 12014 m are obtained by adjusting ψ_0 values using the phase correction $e^{i\omega t}$ as shown in IV.1. Where ω is the angular frequency ($\omega = 2\pi f$) and time $t = \frac{\delta r}{c}$ (δr is the shift in the range of a gun compared to 12000 m and c is the speed of sound in m/s). Table IV.3 shows how the arrays of

pressure values are denoted for different ranges.

$$\psi_1 = \psi_0 e^{-i(2\pi f)(3/1500)}$$
$$\psi_2 = \psi_0 e^{-i(2\pi f)(5/1500)}$$
$$\psi_3 = \psi_0 e^{-i(2\pi f)(7/1500)}$$
$$\psi_4 = \psi_0 e^{-i(2\pi f)(9/1500)}$$
$$\psi_5 = \psi_0 e^{-i(2\pi f)(11/1500)}$$
$$\psi_6 = \psi_0 e^{-i(2\pi f)(14/1500)}$$

The peak amplitude A of an airgun's signature is proportional to the cube root of the volume of air in the airgun. That is $A \sim V^{1/3}$ [7]. Therefore, the volume effects are considered based on the gun volume values in the Table IV.1. Different volumes of the guns are at different positions in the array. The value of the parameter v for a particular far-field distance is calculated as v =sum of number of guns with the same gun volume $\times$ gun volume$^{1/3}$ (see Equation IV.1).

Table IV.3: Arrays of pressure values for guns at different distances

Distance of airguns from the final range (m)	Complex wave arrival from an individual location	Parameter v
12000	ψ_0	v_0=37.7976
12003	ψ_1	v_1=23.2079
12005	ψ_2	v_2=10.0492
12007	ψ_3	v_3=9.5543
12009	ψ_4	v_4=10.7506
12011	ψ_5	v_5=22.9377
12014	ψ_6	v_6=30.5363

$$
\begin{aligned}
v_0 &= 6 * 250^{(1/3)} \\
v_1 &= 5 * 100^{(1/3)} \\
v_2 &= 20^{(1/3)} + 40^{(1/3)} + 60^{(1/3)} \\
v_3 &= 2 * 40^{(1/3)} + 20^{(1/3)} \\
v_4 &= 20^{(1/3)} + 60^{(1/3)} + 70^{(1/3)} \\
v_5 &= 2 * 60^{(1/3)} + 90^{(1/3)} + 2 * 150^{(1/3)} \\
v_6 &= 4 * 150^{(1/3)} + 2 * 100^{(1/3)} \\
\psi &= (v_0 * \psi_0) + (v_1 * \psi_1) + (v_2 * \psi_2) + (v_3 * \psi_3) + (v_4 * \psi_4) + (v_5 * \psi_5) + (v_6 * \psi_6)
\end{aligned}
\tag{IV.1}
$$

Input and output file formats used in the simulations are given in Appendix A. The number of values of ψ in the output file are equal to the product of number of frequencies used in the simulations and number of sea depth values at which ψ are obtained. The values of ψ are weighted by the source spectrum (amplitude as a function of frequency) to obtain sound intensity values as a function of ocean depth and frequency. An inverse Fourier transform was used to get intensity as a function of depth and time.

IV.4 Results and Discussion

Broadband PE sound simulations in the farfield for no shear and shear (bottom with shear speed of 600 m/s) cases with bottom density $\rho = 1600$ kg/m^3, and sound speed in the bottom $c_p = 1700$ m/s are shown in Figures IV.9 and IV.10 respectively.

Also, simulations in the farfield for no shear and shear (bottom with shear speed of 1100 m/s) cases with bottom density $\rho = 2100$ kg/m^3, sound speed in the bottom $c_p = 2200$ m/s are shown in Figures IV.11 and IV.12 respectively. From the figures it is evident that more segments are absent in the cases where the bottom supports shear. Shear speeds of 1100 m/s are not realistic in the Gulf of Mexico. However, the simulations are done for the comparison purposes.

The color bar in Figures IV.9, IV.10, IV.11, and IV.12 is a Decibel scale. Zero value on the color bar indicates the peak intensity value of the time front. All other values in the front are less than the peak value and hence negative values.

IV.5 Conclusion

Simulations are done in a manner that incorporates airgun array geometry. A phase shift method was used to consider the effect of each gun in the airgun array. The bottom structure is shown in IV.4. A broadband source with the center frequency 427.5 Hz was used in the simulations. The acoustic source depth is 7 m. The environment used in the broadband simulations was considered from a previous ocean acoustic airgun experiment [4]. Bottom interaction of the sound is taken into account. Acoustic intensity values are calculated at a horizontal range (12 km).

Convergence testing was performed using different range and grid parameters. The correct combination of computational grid parameters were found. Results from the convergence testing show that different grids must be used to simulate low and high frequency broadband simulations. Low frequency sound (which has longer wavelengths) must use a relatively high value of range step and high frequency sound (which has smaller wavelengths) must use a lower value of range step.

Considering all the environmental complexities, bottom interacting sound was successfully modeled using the CD equivalent parameters obtained for both soft and hard bottom cases. From the figures, the effects of shear are noted. The broadband PE fronts for the soft bottom (with $c_s = 600$ m/s) has a significant impact due to shear loss. This can be seen in Figures IV.9 and IV.10. Although the sea bottom with shear speed $c_s = 1100$ m/s is not realistic in the Gulf of Mexico region, broadband simulations were performed for the hard bottom case to see the impact of shear loss. From Figures IV.11 and IV.12, it is clearly noted that shear impact is high in hard bottom case.

Improvement in source signature can be done. Sound propagation simulations are possible with the EEF method even when there are complicating environmental factors such as range-dependent bottom, bottom interactions, shallow source depth (7 m), high centered frequency, ($f_c = 427.5$ Hz) and a wide frequency band.

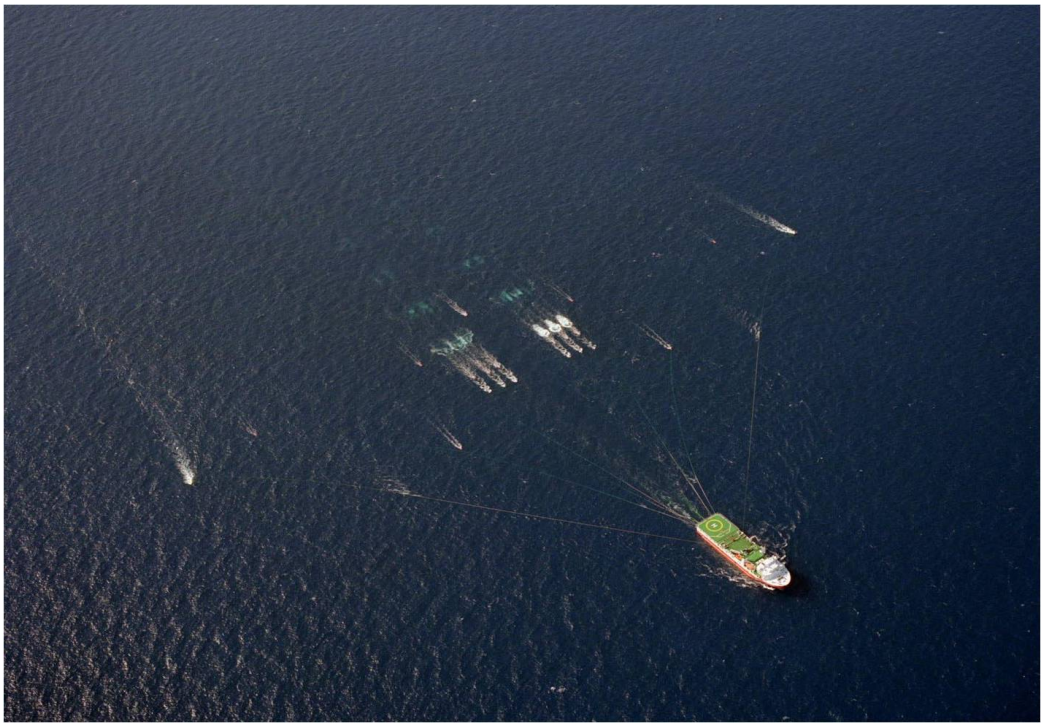

Figure IV.1: This figure shows a seismic survey ship with airguns towed behind it. Currently, most of the seismic surveys involved in the exploration of hydrocarbon are using arrays of airguns as the source of seismic signals. This figure is considered from an overview of marine seismic operations by International Association of Geophysical Contractors [6].

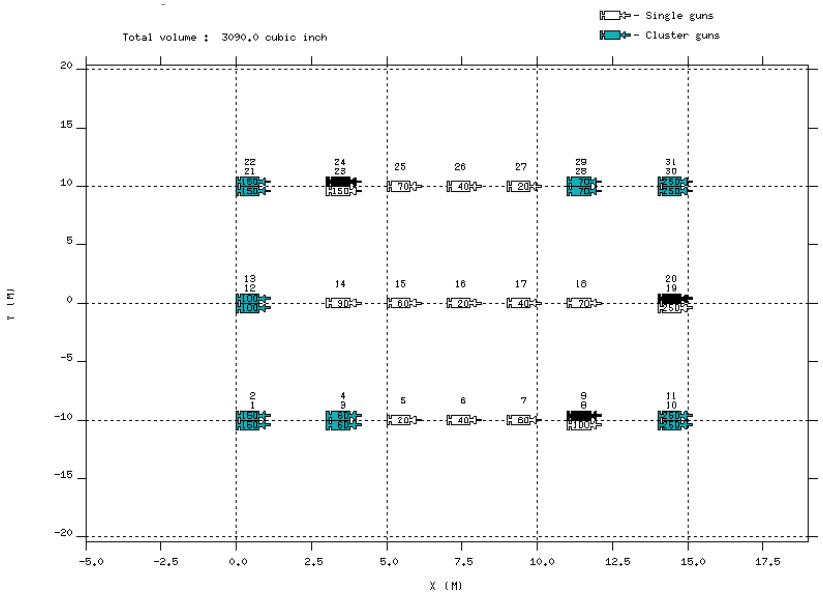

Figure IV.2: An example of a size of airgun array with a total of 31 guns is shown in the figure. It is a two dimensional array with 15 m$\times$20 m. Some of the guns are individual and some are clusters (consisting of more than a single gun). The gun array geometry was obtained through personal communication with Dr. James Stephens.

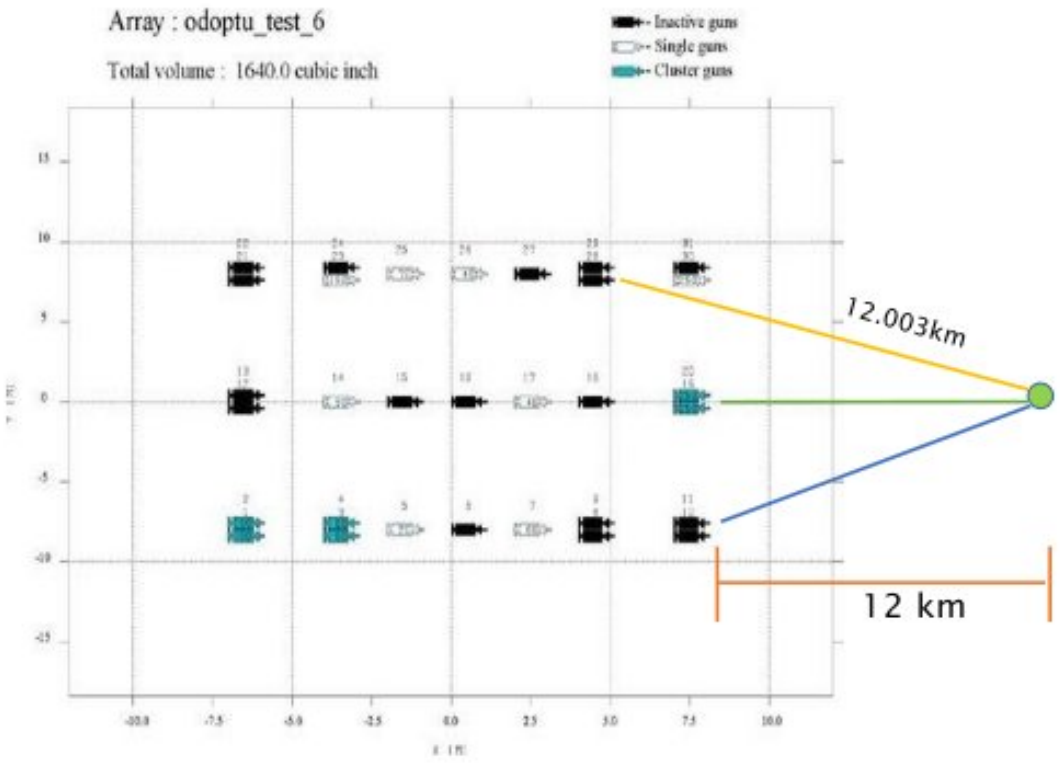

Figure IV.3: This figure shows how individual guns are at different positions from the receiving point in the farfield (12 km from the middle gun in the right most column of guns).

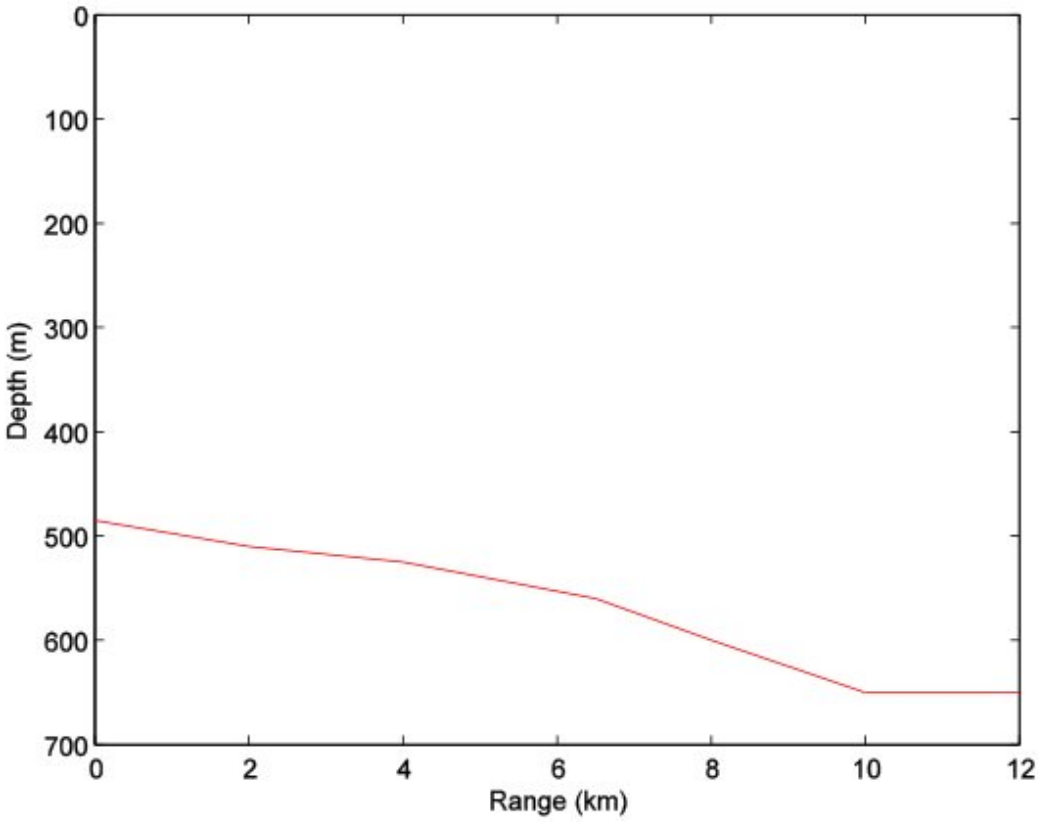

Figure IV.4: The red line shows the sea bottom variation as a function of range in the west Mississippi canyon region. The water depth varies from 400 to 800 m with a bathymetric slope of 1.5° [4].

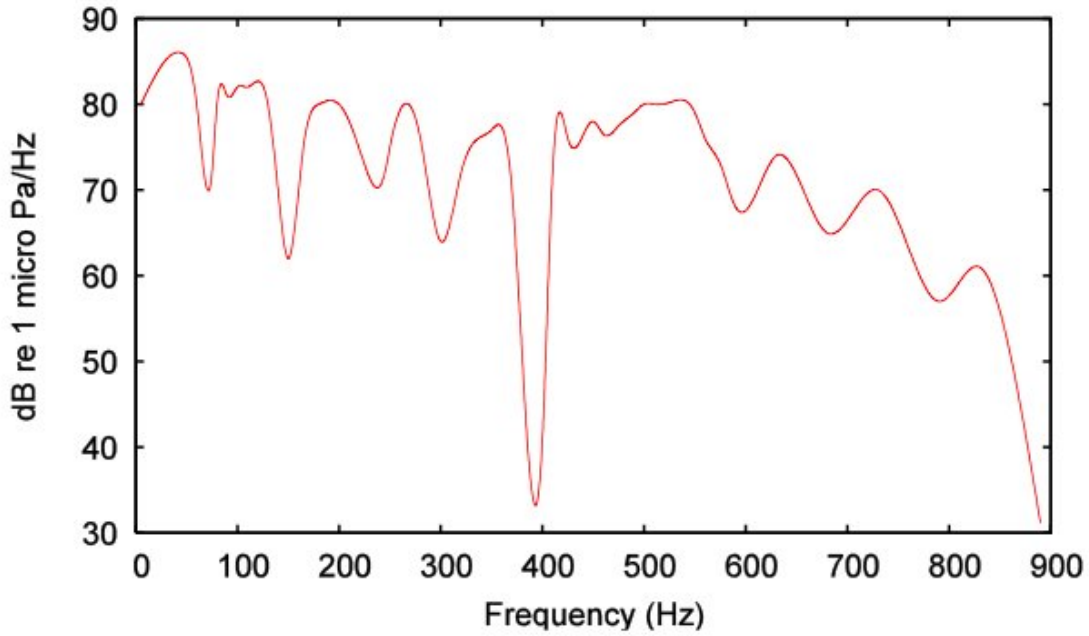

Figure IV.5: The figure shows a horizontal airgun array amplitude spectrum at 1000 m range from a source. The horizontal amplitude spectrum has less strength compared to the vertical amplitude spectrum. This is because most of the seismic energy from the airgun array is directed vertically downward. This spectrum was plotted based on a figure in the paper "Airgun Arrays and Marine Mammals" by International Association of Geophysical Contractors [7].

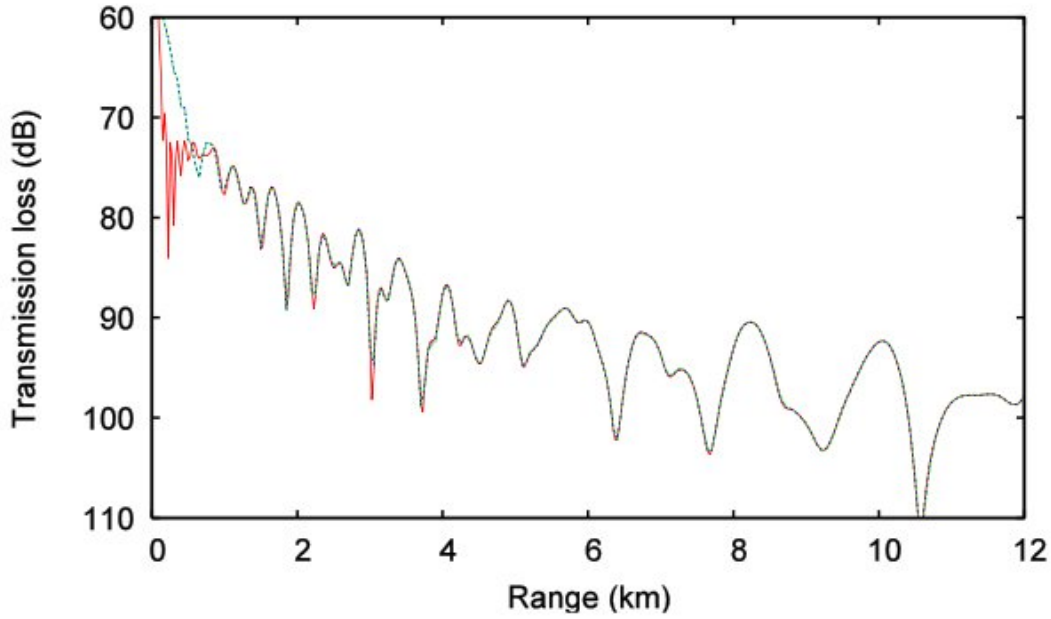

Figure IV.6: Transmission loss (dB) as a function of range (km) is plotted for a frequency of 20 Hz. The bottom with density $\rho = 1700$ kg/m^3, sound speed in the bottom $c_p = 1700$ m/s and shear speed $c_s = 0$ m/s (shear ignored in the bottom) was used. Simulation with computational grid depth step dz= 0.5 m and range step dr= 25 m is shown in red, dz= 1 m, dr= 50 m in green, and dz= 0.5 m, dr= 50 m in blue.

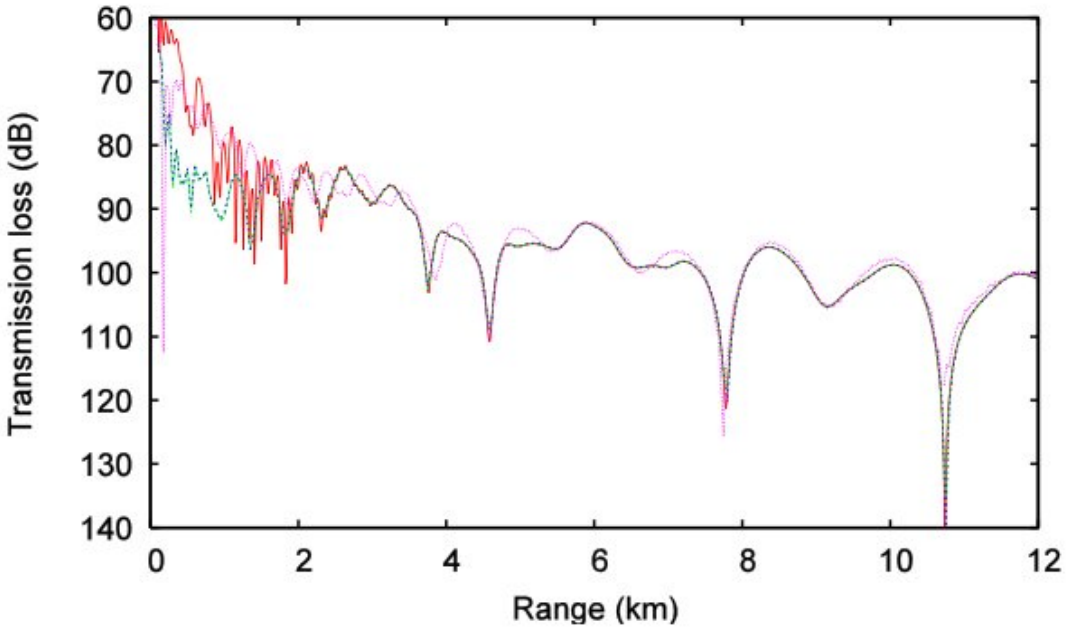

Figure IV.7: Transmission loss (dB) as a function of range (km) is plotted for a frequency of 20 Hz. The bottom with density $\rho = 1700$ kg/m^3, sound speed in the bottom $c_p = 1700$ m/s and shear speed $c_s = 600$ m/s was used. Simulation with computational grid depth step dz= 0.5 m and range step dr= 10 m is shown in red, dz= 0.5 m, dr= 50 m in green, dz= 1 m, dr= 50 m in blue, and OASES curve in magenta.

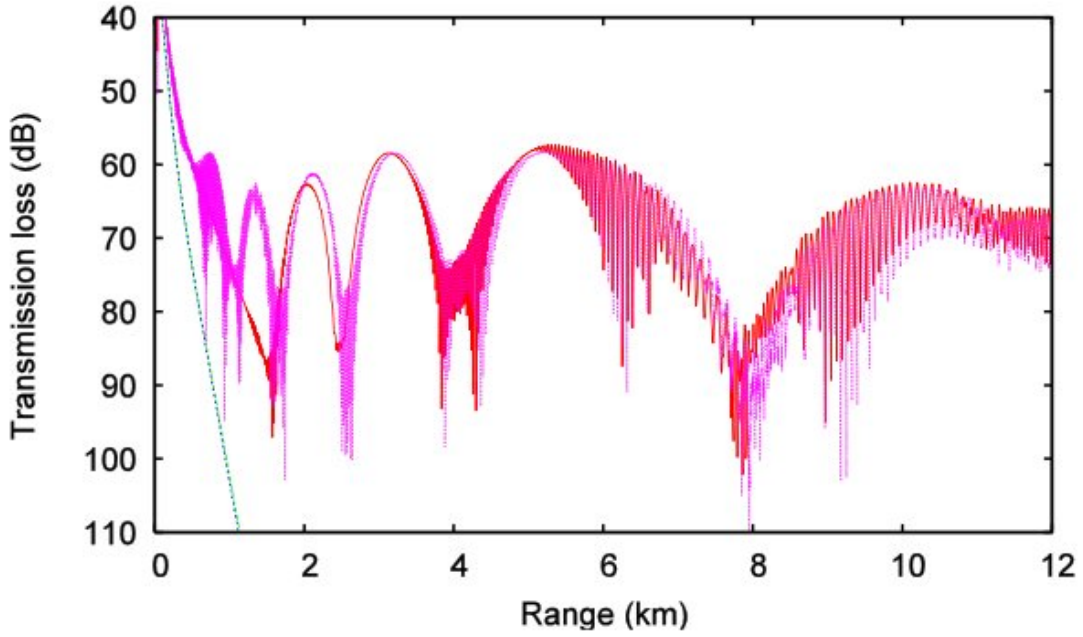

Figure IV.8: Transmission loss (dB) as a function of range (km) is plotted for a frequency of 600 Hz. The bottom with density $\rho = 1700$ kg/m^3, sound speed in the bottom $c_p = 1700$ m/s and shear speed $c_s = 600$ m/s was used. Simulation with computational grid depth step dz= 0.5 m and range step dr= 5 m is shown in red, dz= 0.5 m, dr= 50 m in green, dz= 1 m, dr= 50 m in blue, and OASES curve in magenta.

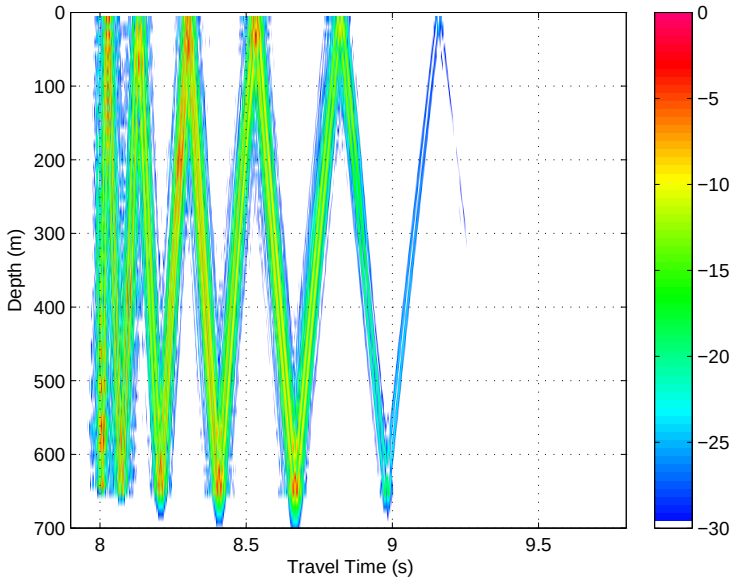

Figure IV.9: This figure shows the wavefronts reflected off of a soft bottom where shear is ignored. The bottom density is $\rho = 1600$ kg/m^3; sound speed in the bottom is $c_p = 1700$ m/s.

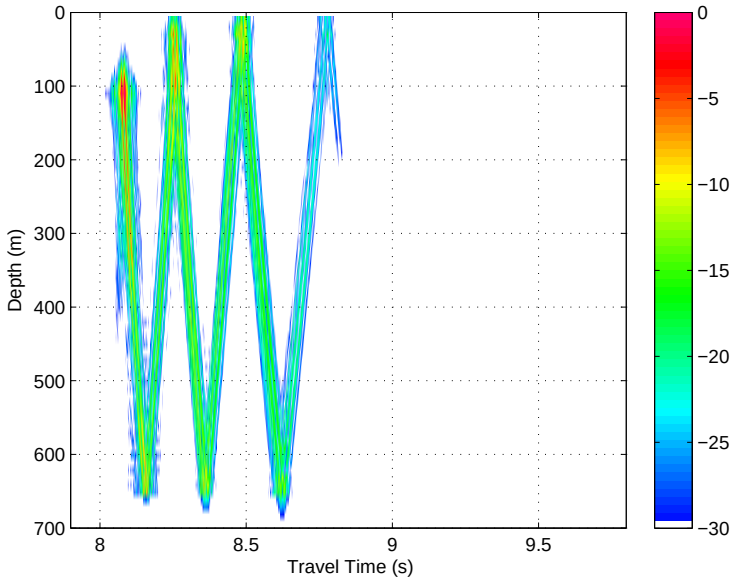

Figure IV.10: Wavefronts in the figure have bottom interacted and suffered a shear loss. The bottom has a shear speed of 600 m/s. The bottom density is $\rho = 1600$ kg/m^3; sound speed in the bottom is $c_p = 1700$ m/s.

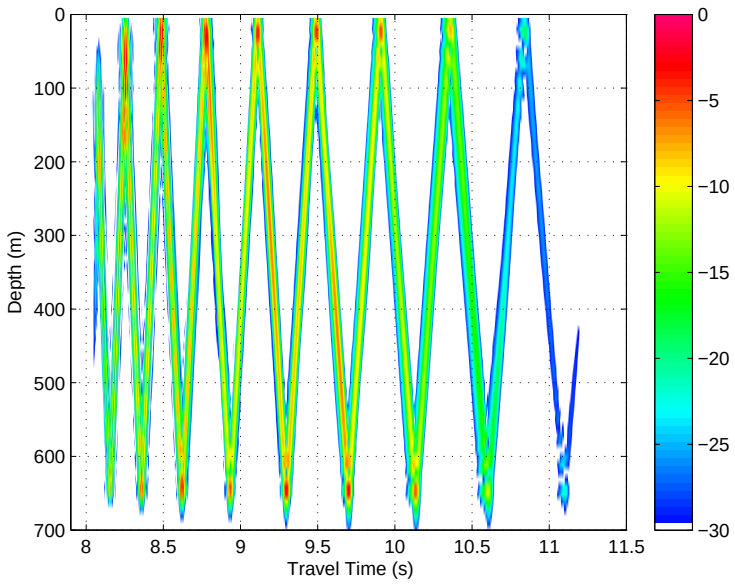

Figure IV.11: This figure shows the wavefronts reflected off of a hard bottom where shear is ignored. The bottom density is $\rho = 2100$ kg/m^3; sound speed in the bottom is $c_p = 2200$ m/s.

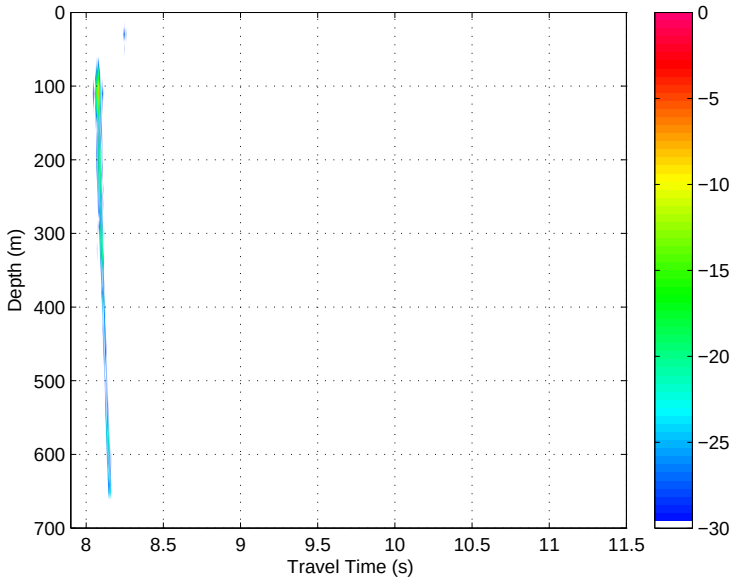

Figure IV.12: Wavefronts in the figure are bottom interacted and suffered a significant amount of bottom loss. The loss is much higher than in Figure IV.11. The bottom has a shear speed of 1100 m/s. The bottom density is $\rho = 2100$ kg/m^3; sound speed in the bottom is $c_p = 2200$ m/s.

Chapter V

AN APPLICATION OF THE EEF METHOD BASED ON BASSEX

V.1 Introduction

BASSEX stands for Basin Acoustic Seamount Scattering EXperiment. BASSEX was conducted to understand the effect of bottom interactions and to investigate the propagation of the sound field as it travels downslope into deep water. This experiment was conducted using the North Pacific Acoustic Laboratory (NPAL) source located near Kauai, Hawaii. The acoustic source depth is 810.90 m. A portable receiver array was used to record the transmissions at a range of 3.59 km from the acoustic source. The sea bottom near the source is very steep due to its volcanic origins as shown in Figure V.1. A high-fidelity 200 m horizontal line array was used near the source to evaluate the signal at various ranges and azimuths. Received data shows that sound energy was reflected from the seafloor near the source. The aim of this study is to estimate the seafloor parameters (density, sound speed in the bottom and shear speed) using the received data. This is a geoacoustic inversion process.

Acoustic reflections off of a steep volcanic island are a severe challenge to ocean-acoustic models. This is a strongly range-dependent environment. Parabolic-equation modeling is a good choice for this environment. The seafloor in this region is basalt, which supports shear waves. However, the computational stability of the elastic parabolic equation is a challenge due to severe down slopes and the hard sea bottom. Equivalent fluids generated by treating the sound speed in the bottom c_p, shear speed c_s, and density ρ as free parameters (the EEF method) have been shown to effectively model the sound which has suffered shear losses due to sea bottom interaction [22]. The Zhang and Tindle method uses only an effective density and does not change the actual bottom sound speed. This method is useful only when a low grazing angle interval is relevant and when shear is a relatively small contributor to acoustic loss [21].

V.2 Method

A complex-density (CD) equivalent fluid that results in the best correspondence between acoustic simulations and the experimental data was found through a brute-force search process [5]. This search process tries all values in the given search range and finds the best combination of CD

equivalent fluid values. Equivalent fluids can be used to mimic the elastic solids in acoustic simulations. Sound waves which have interacted with the seafloor can be modeled by using equivalent fluids in acoustic simulations. In order to determine the actual elastic seafloor for which the CD equivalent fluid is an effective representative, a brute-force search is performed. A brute-force search means that every combination in the given range of values will be used in the search to find a best match. Reflection coefficients resulting from all discrete values for each of the parameters within a specified interval are compared to the equivalent fluid. Using the brute force technique, the feasibility of finding the estimated values of the elastic bottom parameters for a volcanic seafloor from the CD equivalent fluid is investigated.

V.3 Finding Elastic Bottom Parameters

A 75 Hz center frequency broadband acoustic source was used in this experiment. The source is bottom mounted. So modeling the experimental receptions must take acoustic interaction with the seafloor into consideration. Additionally, the bottom material in this region has volcanic composites. This suggests that the generation of elastic shear waves in the seafloor could show a high influence on the sound reflected back into the water column. The use of a CD equivalent fluid to characterize the impact of an elastic bottom without detailed modeling of the induced shear components can improve computational efficiency and stability. Using the CD equivalent fluid in a previous effort to simulate acoustic arrivals from this source at a range of 3890 km yielded a sound field that is similar to the experimental data in the long-range NPAL experiment. So the acoustic arrivals from the simulations are unambiguously identified with those from the long-range data [22].

A reception from the BASSEX data selected for this analysis is shown in blue and simulation is shown in red in Figure V.2. The receiver is at a range of 3.59 km and at a depth of approximately 260 m. According to the ray calculations, the relevant trajectories between $2.4-2.6$ seconds arrival include both non-bottom-interacting paths and paths that interact with the bottom (reflect from the bottom near the source). The sound arriving at travel times between 3.0 and 3.4 s corresponds only to the rays which have reflected from the bottom. Also the intensity level of this sound is roughly 15 dB less than the earlier arrival.

Parabolic-equation simulations for the 3.59 km range were performed for a range of different CD equivalent fluids. Bottom parameters included 20 values of the compressional speed c_p (from 1000 to 4800 m/s), and 14 values each for the real and imaginary parts of the effective density ρ'_R, ρ'_I (from 200 to 2800 kg/m^3) for a total of 3920 cases. Attenuation in the bottom is

taken to be 0.5 dB/λ in all cases. The bathymetry was taken from a survey of the source area associated with the North Pacific Acoustic Laboratory experiment [38]. The simulation results were compared to the received level data based on the cost function

$$C_A = \frac{1}{N_i}\Sigma_{t_i}|D(t_i) - S(t_i)| \tag{V.1}$$

where t_i are the times for which the simulated level $S(t)$ exceeded -30 dB below maximum, $D(t_i)$ and $S(t_i)$ are the data and simulation levels in dB, and N_i is the number of included values. This cost function gives the average difference in the intensity between the sound obtained in data and simulation as a function of time. The smallest value of C_A was found for an effective sound speed of 4200 m/s and an effective complex density of $400 + i1200$ kg/m^3. The data and simulation results for the reflected arrival are shown in Figure V.2.

The best CD equivalent-fluid obtained can be used to estimate the actual elastic parameters of the solid seafloor. Ray analysis was performed to find the relevant grazing angle interval for which the CD equivalent fluid and the elastic solid should have similar reflection coefficients. This analysis is also used to point out that the sound energy between 2.4 and 2.6 s corresponds to both direct arrivals and near-source bottom reflections. Ray analysis was done for launch angles every 0.5° between $\pm 75°$. The bathymetry along the sound propagation path and the histogram of the grazing angles for their reflections are shown in Figure V.4. Using the histogram, the relevant grazing angle interval obtained is 25°-65°.

Elastic bottom parameters can be estimated from the equivalent fluid that best reproduces the data. A brute-force technique is used to determine the bottom parameters from the CD equivalent fluid parameters. In this technique, the real and imaginary part of complex density and the sound speed in the bottom are given as input to a code which searches for a set of bottom parameters (density, sound speed in the bottom, and shear speed) whose reflection coefficient (RC) best matches with the RC of the CD equivalent fluid. The best match between the given equivalent fluid and an elastic solid was based on the cost function given below,

$$C_v = \frac{1}{N_i}\Sigma_{\theta_i}\frac{|V_{es}(\theta_i) - V_{ef}(\theta_i)|}{V_{es}(\theta_i)} \tag{V.2}$$

where θ_i are the set of integer angles from $25° - 65°$, N_i is the number of such angles, and V_{es} and V_{ef} are the reflection coefficients for the elastic solid and the CD equivalent fluid respectively [5].

V.4 Results and Discussion

The seafloor near Kauai, Hawaii is very hard due to its volcanic origins. The bottom parameters obtained in the brute-force technique are density $\rho = 2040$ kg/m^3, sound speed in the bottom $c_p = 2300$ m/s, shear speed $c_s = 1000$ m/s. The results obtained using the brute-force technique are roughly comparable to an initial estimate of the elastic parameters made in this area. The estimated elastic parameters of the bottom in the Kauai region are density $\rho = 2100$ kg/m^3, compressional speed $c_p = 2200$ m/s and shear speed $c_s = 1100$ m/s [22].

Figure V.5 shows the bottom loss (BL) in decibels plotted against grazing angle for both the CD equivalent fluid (red) and elastic bottom (green) obtained using the brute-force technique. Although the BL curves are notably different, it can be seen in the figure that the BL from the elastic bottom captured the important reflection characteristics at the necessary grazing angles of a hard bottom. For a single frequency of 75 Hz, transmission loss (in dB) as a function of range (in km) for the brute-force resulted elastic bottom (green) and CD equivalent fluid (red) is shown in V.6. A benchmark code (RAMS) was used to plot the transmission loss line for the elastic bottom. The red and green lines are matched very well with a very small discrepancy.

Parabolic equation multi-frequency simulations were performed using both equivalent fluid and the elastic bottom (see Figures V.3 and V.7). Both figures use the same value of peak absolute intensity (5.6658×10^{-05}) to normalize the wave function for comparison purpose.

V.5 Conclusion

In this study, a geoacoustic inversion is performed using short-range transmissions over steep bottom with volcanic material. This kind of bottom is expected to support shear waves (speeds ranging from several hundred meters per second to several thousand). The effective shear speed was estimated using the CD equivalent model in parabolic-equation simulations. CD equivalent fluids have shown to effectively model the bottom interacting sound. The equivalent fluid that produced the best match of arrival time and amplitude to the measured data is found from a search process based on Equation V.1. In the search process, multi-frequency simulations were performed using a total of 3920 CD equivalent fluids. The CD of the fluid that was obtained from the search process is $400 + i1200$ kg/m^3 and the effective compressional speed is 4200 m/s. The grazing angle interval used was $25^\circ - 65^\circ$. An inversion is performed to find the elastic bottom parameters using the CD equivalent fluid. Determining the elastic bottom parameters of the seafloor using the experimental data involves the use of CD equivalent fluid. The resulting elastic bottom values are density $\rho = 2040$ kg/m^3, sound speed in the bottom $c_p = 2300$ m/s,

and the shear speed $c_s = 1000$ m/s. These steps involved in the geoacoustic inversion are shown in a chart form in Figure V.8.

This study proves one of the important applications of the CD equivalent fluids. The brute-force technique can be used to find an unknown elastic bottom values using the CD equivalent fluid representing a particular seafloor.

There are significant advantages using the geoacoustic inversion discussed in this chapter. Simulations using the CD equivalent fluids are simple and quick. Broadband simulations for many cases can be reliably done in a complex environment type like BASSEX. The results achieved in this chapter convey that it is possible to back track elastic bottom parameters using CD equivalent fluid parameters. Limitations of geoacoustic inversion are (a) uniqueness of of the result is not known at this point. (b) Using this inversion process, it is only possible to approximate an effective representative of an actual elastic bottom.

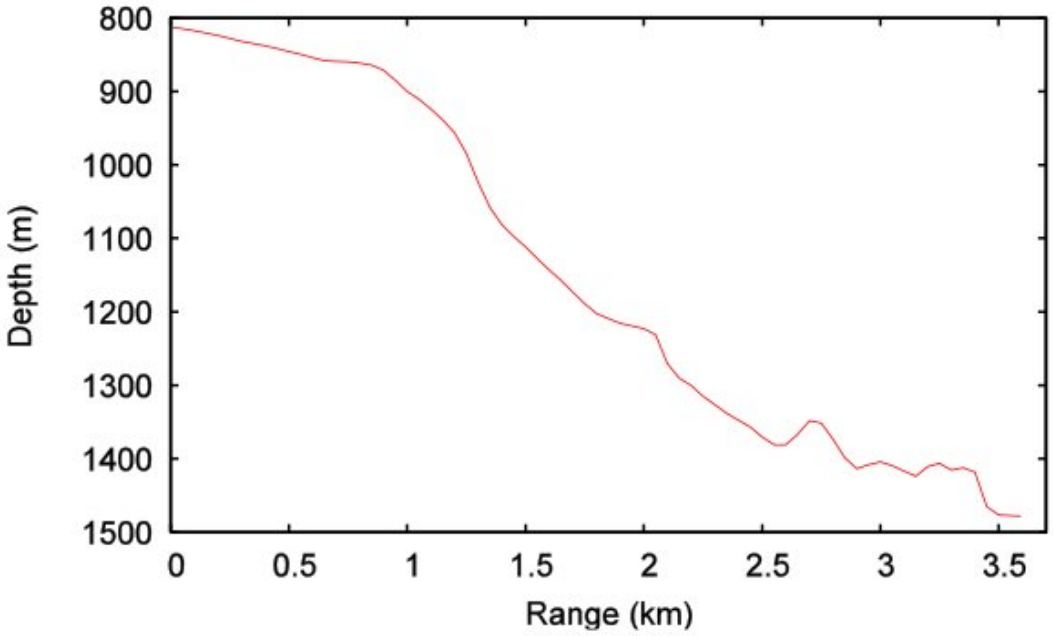

Figure V.1: The bathymetry (depth variation of the seabed with range) of the BASSEX for a range of 3.59 km is shown in the above figure. The bottom is very steep near the source. The varying bottom made the environment highly range-dependent. The source is at 810.90 m depth.

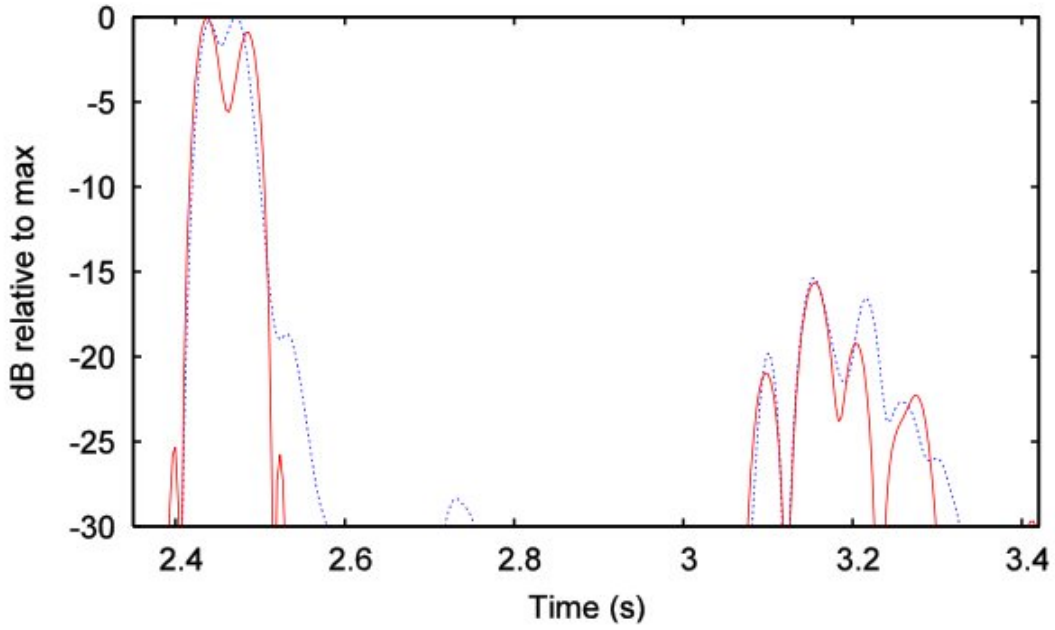

Figure V.2: The above figure shows the intensity of the signal as a function of time obtained at a range of 3.59 km. The experimental received level is shown as a blue line. Comparison with ray calculations has shown that the energy between 2.4 and 2.6 seconds corresponds to both purely water-borne and reflected rays. The arrival energy between 3.0 and 3.4 seconds consists only from bottom reflected rays. Results from a simulation using a CD equivalent fluid for the ocean bottom are shown as a red line [5].

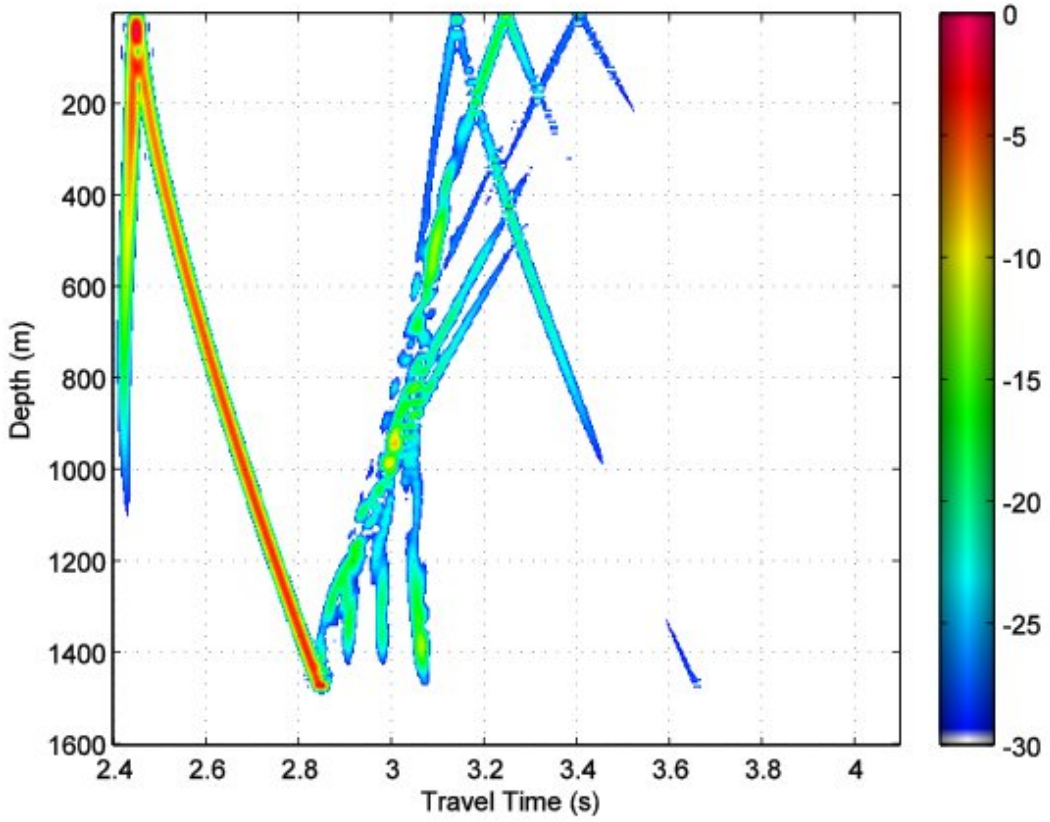

Figure V.3: This is a broadband parabolic equation simulation using the CD equivalent fluid $\rho' = 400 + i1200$ kg/m^3 and $c'_p = 4200$ m/s. A broadband source with 75 Hz center frequency was used. The source depth is 810.90 m. The figure shows the wavefronts as a function of depth and time. The highest value in the color bar indicates the peak value of the intensity in the plot.

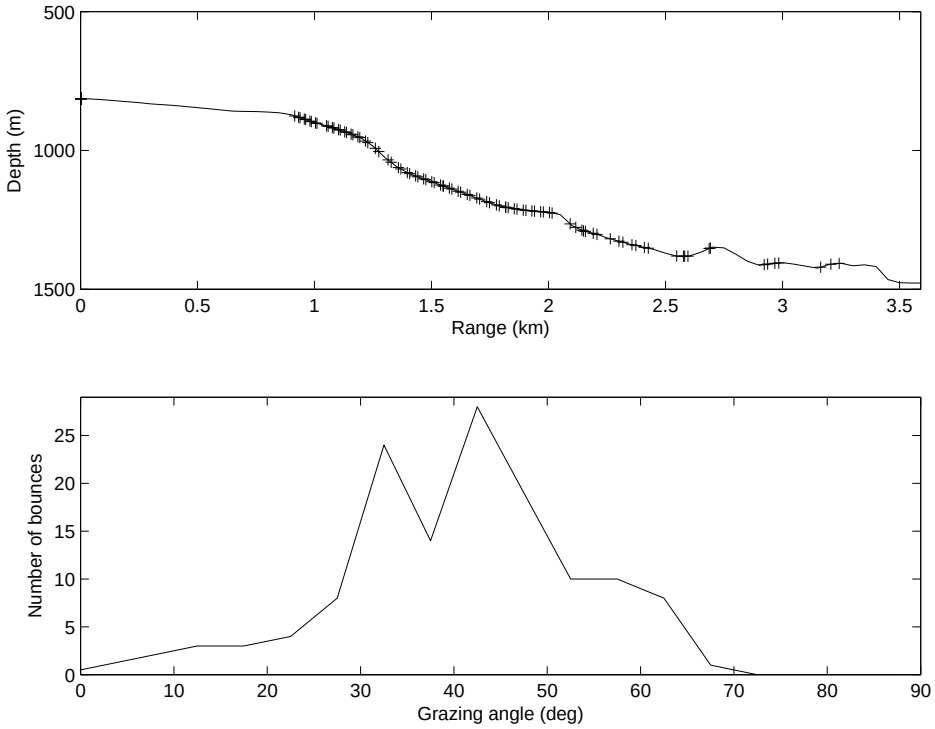

Figure V.4: The top panel depicts both the seabed structure (line) and the reflection location (crosses) of the 135 sample rays with travel times between 3.0 and 3.4 seconds at a range of 3.59 km. The bottom panel shows the number of ray bounces as a function of grazing angle θ_z within 5° bins. This figure was considered from "Geoacoustic inversion for a volcanic seafloor using equivalent fluids" [5].

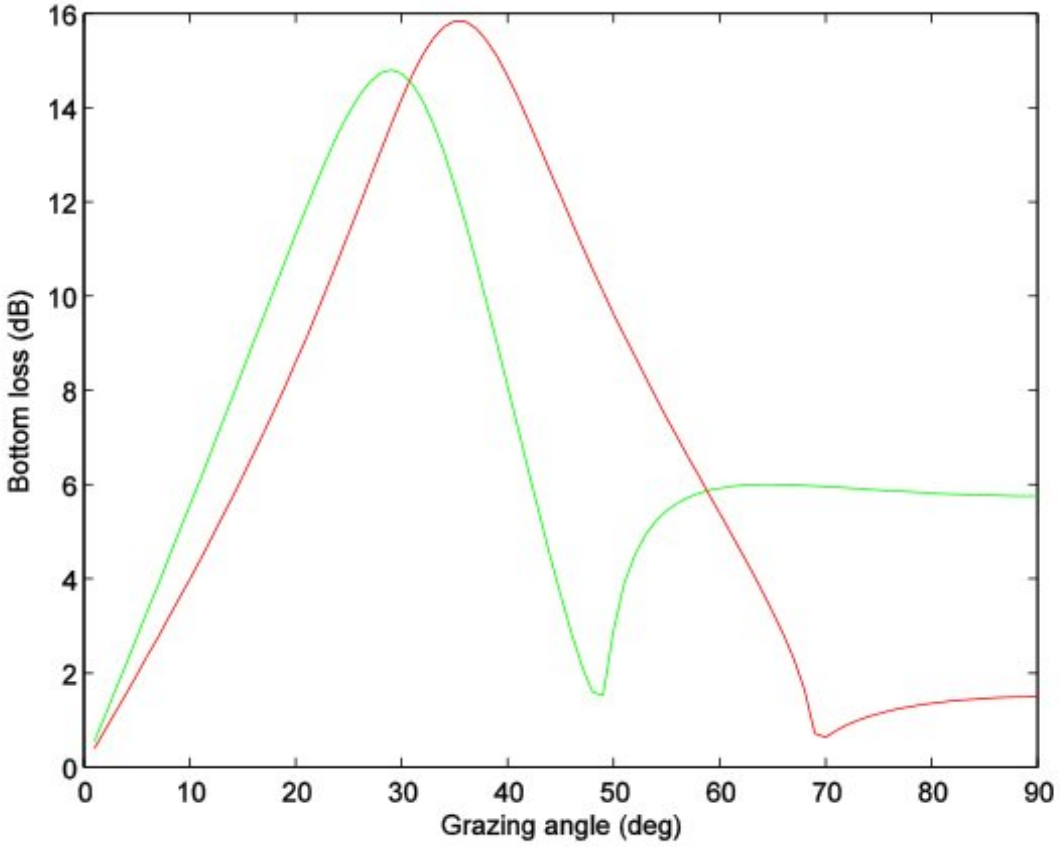

Figure V.5: Bottom loss ($BL = -10\log|V|^2$ in decibels) variation as a function of grazing angle θ_z is shown for both the equivalent fluid that best represents the seabed (red) and the elastic bottom parameters obtained using brute-force technique (green).

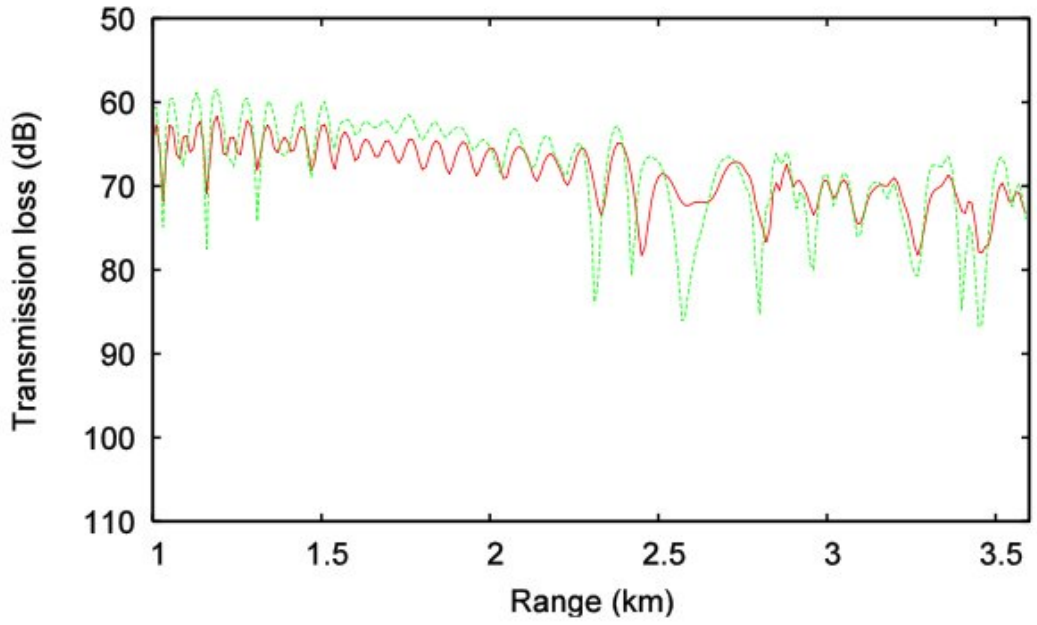

Figure V.6: Transmission loss (TL) comparison is shown as a function of range in kilometers for a frequency of 75 Hz. TL curve for the elastic bottom obtained from brute-force technique ($\rho = 2040$ kg/m^3, $c_p = 2300$ m/s and $c_s = 1000$) is shown in green and the red curve is the TL due to equivalent fluid ($\rho' = 400 + i1200$ kg/m^3, $c'_p = 4200$ m/s).

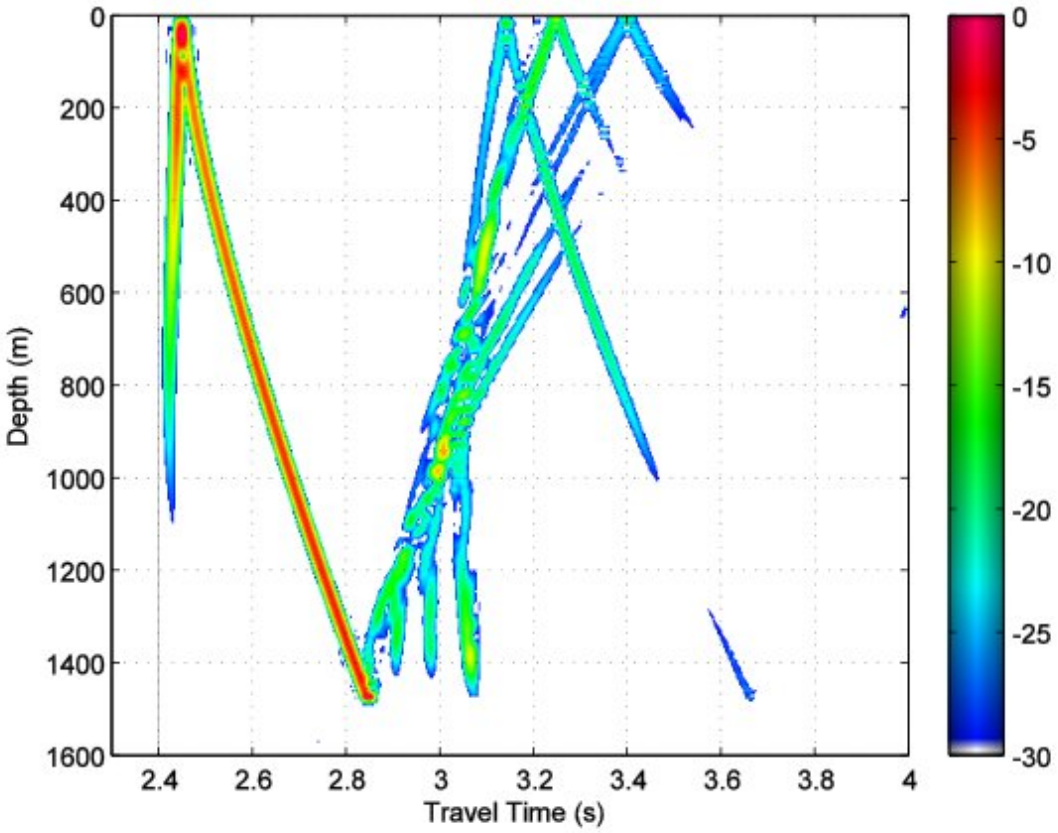

Figure V.7: This is a broadband parabolic equation simulation using the brute-force technique outcome of elastic bottom parameters (density $\rho = 2040$ kg/m^3, sound speed in the bottom $c_p = 2300$ m/s, and the shear speed $c_s = 1000$ m/s). The total number of frequencies simulated was 301.

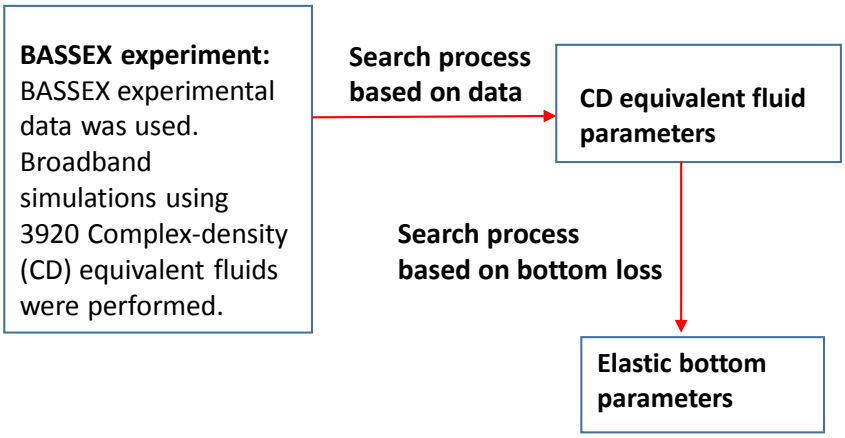

Figure V.8: This chart illustrates the steps involved in the process of calculating an estimate of the elastic bottom parameters from BASSEX experimental data recordings.

Chapter VI

SUMMARY

This dissertation is divided into three parts which are explained in the following paragraphs. The first part explains the background, flexibility, and limitations of the Expanded Equivalent Fluid (EEF) method. The second part discusses the ability and advantages of the EEF method in simulating bottom interacting sound in different environments. In this part, simulation results obtained using the EEF method were compared with the benchmark results (OASES, RAMS) and to the results obtained from a previous equivalent fluid technique called the Zhang and Tindle method. In part three, application of the EEF method in two different environments is discussed.

Part 1: The reflection coefficient of a soft solid seabed with a low shear speed can be well approximated by replacing the sea floor with an equivalent fluid of suitably chosen parameters. This is called an equivalent fluid approximation. This technique was developed by Zhang and Tindle [21]. An equivalent fluid employs parameters of the sea bottom often including Complex-Density (CD) whose reflection coefficient best matches with the reflection coefficient of an elastic bottom. The Zhang and Tindle (ZT) method works well for the simulation environments where low grazing angle intervals are relevant. This technique was expanded to also perform well in cases where higher grazing angle intervals are relevant. This method is called the EEF method. When a relevant grazing angle interval, bottom parameters (density ρ, sound speed in the bottom c_p, and shear speed c_s) are provided as inputs, the EEF method produces a CD equivalent fluid ($\rho' = \rho'_R + i\rho'_I$) and an effective sound speed in the bottom c'_p as output. The EEF method has one more free parameter (sound speed in the bottom c_p) compared to the ZT method. This method also has the flexibility to use a desired grazing angle interval (In the BASSEX example in Chapter V, the relevant grazing angle interval is $25^\circ - 65^\circ$). Both methods (the EEF and ZT) are unable to simulate sound which has interacted with a sea bottom with very high shear speed c_s. An example of a hard bottom discussed is in Chapter III. See Figure III.11. For very wide grazing angle intervals, the EEF method fails for some media.

Part 2: In Chapter III, the efficiency of the EEF method was tested in different simulation environments. The EEF method was used to obtain a CD equivalent fluid for a particular set of elastic bottom parameters. The EEF method is very efficient in simulating bottom interacting

sound. Based on the Transmission Loss (TL) results, the method can be applied to sea bottom environments with high shear speeds (for example, NPAL TL in Chapter III). This method can be applied in cases where higher grazing angle intervals are relevant (for example, the BASSEX case in Chapter V). The performance of the EEF method was proved by showing several examples of the acoustic TL in different environments such as NPAL, BASSEX, soft bottom, and hard bottom cases. The EEF simulation results were compared to the benchmark models (OASES and RAMS) and the ZT method results.

Part 3: Using the CD equivalent fluid parameters obtained from the EEF method, farfield simulations of sound from an array of airgun sources were successfully performed. Considering the airgun array geometry, sound at 12 km range was simulated. A phase shift method was used to consider the effect of each airgun in the array. The simulation environment considered was from a previous ocean acoustic experiment which used an array of airguns as the acoustic source (details of the environment were explained in Chapter IV). Sound in this environment interacts with the sea bottom. CD equivalent fluids generated using the EEF method were used to model the bottom interacting sound. Broadband parabolic equation simulations were performed by considering the seafloor shear effects for the soft and hard bottom cases. These results were compared to the simulations results which were performed by ignoring the shear in the seafoor. Chapter IV provides broadband simulation results of sound from an array of airgun sources in the farfield. Comparison between no shear and shear cases clearly shows the difference in intensity levels. Sound energy loss to shear is significant when compared to cases without shear.

Geoacoustic inversion was performed to find the elastic bottom parameters for an elastic seafloor. This is another instance where the application of the EEF technique is significant. The Basin Acoustic Seamount Scattering EXperiment (BASSEX) was conducted to understand the effect of bottom interactions and to investigate the propagation of the sound field as it travels downslope into deep water. A complex-density (CD) equivalent fluid that results in the best correspondence between acoustic simulations and the experimental data was found through a search process [5]. For a total of 3920 CD equivalent fluids, acoustic broadband simulations were performed in this search process. A relevant grazing angle interval in this environment, $25^\circ - 65^\circ$, was found through ray analysis. The EEF method produced successful acoustic acoustic simulations in this case. The ZT method is not applicable in this environment because of the high grazing angle interval. Using a brute-force technique, an estimate of the elastic bottom parameters were found from the CD equivalent fluid parameters.

Simulations were performed using codes written in the FORTRAN 77 computer language. Broadband PE simulation plots were obtained using MATLAB.

Appendix A

PERAMCD SIMULATIONS

A.1 PERAMCD input file format

An example of PERAMCD input file is presented below.

```
# Bottom parameters (maximum depth,depth step size, and depth sampling rate)
1000.0
0.5
20
# Source and attenuation parameters (acoustic source depth, depth value at which attenuation
#starts, attenuation value, and Pade coefficients)
7.0
950.0  30.0
4  2  0.0
# Range parameters (range, range step size, range sampling rate,
# how many range output files, output range, and output file)
12000.0
50.0
5
1
12000.0
'psi.output.dat'
# Sound speed profile (number of values in SSP, perturbations, SSP file,
# perturbation file, number of bathymetry values, and bathymetry file)
2048  10.0
'ctd4_1prf2048f.ss'
'none'
7
'bath_drter.dat'
# Bottom parameters (complex-density density real part, imaginary part,
effective sound speed in the bottom, and attenuation value)
0.8519
0.1280
1703.8
0.5
# Frequency information (center frequency, band width, time window,
# starting frequency, and ending frequency)
427
423
4
4
0
```

BIBLIOGRAPHY

[1] E. L Hamilton. Elastic properties of marine sediments. *Journal of Geophysical Research*, 76:579–604, January 1971.

[2] M D Vera. Examples and applications in long-range ocean acoustics. *European Journal of Physics*, 28:1063–1072, September 2007.

[3] Jerald W. Caruthers. *Fundamentals of Marine Acoustics*. Elsevier Scientific Publishing Company, 1977.

[4] Stacy L. DeRuiter, Peter L. Tyack, Ying-Tsong Lin, Arthur E. Newhall, James F. Lynch, and Patrick J. O. Miller. Modeling acoustic propagation of airgun array pulses recorded on tagged sperm whales. *Journal of the Acoustical Society of America*, 120:4100–4113, 2006.

[5] Kevin D. Heaney, Michael D. Vera, and Arthur B. Baggeroer. Geoacoustic inversion for a volcanic seafloor using equivalent fluids. Collaborative work, in preparation.

[6] Marine seismic operations. International Association of Geophysical Contractors, March 2002. An Overview.

[7] Airgun arrays and marine mammals. International Association of Geophysical Contractors, August 2002.

[8] Appeltans W, Bouchet P, Boxshall GA, De Broyer C, de Voogd NJ, Gordon DP, Hoeksema BW, Horton T, Kennedy M, Mees J, Poore GCB, Read G, Stöhr S, Walter TC, and Costello MJ. World register of marine species, August 2013.

[9] Alan Gianmbattista, Betty McCarthy Richardson, and Robert C. Richardson. *College PHYSICS*. McGraw-Hill, 2004.

[10] J. A. DeSanto. *Ocean Acoustics*. Springer-Verlag Berlin Heidelberg, 1979.

[11] Clay Clarence S. and Medwin Herman. *Acoustical Oceanography*. A Wiley-Interscience Publication, 1977.

[12] Xavier Lurton. *An Introduction to Underwater Acoustics Principles and Applications*. Springer-Verlag Berlin Heidelberg, 2010.

[13] L. Brekhovskikh and Yu. Lysanov. *Fundamentals of Ocean Acoustics*. Springer-Verlag Berlin Heidelberg, 1982.

[14] C. B. OFFICER. *Introduction to the Theory of SOUND TRANSMISSION with Application to the Ocean*. McGraw-Hill, 1958.

[15] V. A. Del Grosso. New equation for the speed of sound in natural waters (with comparisions to other equations). *Journal of the Acoustical Society of America*, 56:1084–1091, 1974.

[16] Stanley M. Flatté and Michael D. Vera. Comparison between ocean-acoustic fluctuations in parabolic-equation simulations and estimates from integral approximations. *Journal of Acoustical Society of America*, 114:697–706, August 2003.

[17] Stanley M. Flatté, Roger Dashen, and Walter H. Munk. *Sound Transmission Through a Fluctuating Ocean*. Cambridge University Press, 1979.

[18] Richard Phillips Feynman, Robert Benjamin Leighton, and Matthew Linzee Sands. *Feynman Lectures on Physics*. California Institute of Technology, 1963.

[19] Martin H. Schultz and Ding Lee. *Computational Ocean Acoustics*. Pergamon Press Ltd., 1985.

[20] Ivan Tolstoy and C. S. Clay. *OCEAN ACOUSTICS Theory and Experiment in Underwater Sound*. American Institute of Physics, 1987.

[21] Z.Y. Zhang and C.T. Tindle. Improved equivalent fluid approximations for a low shear speed ocean bottom. *Journal of the Acoustical Society of America*, 98:3391–3396, 1995.

[22] Michael D. Vera and Kevin D. Heaney. The effect of bottom interaction on transmissions from the North Pacific Acoustic Laboratory Kauai source. *Journal of the Acoustical Society of America*, 117:1624–1634, 2005.

[23] F.B. Jensen, W.A. Kuperman, M.B. Porter, and H. Schmidt. *Computational Ocean Acoustics*. American Institute of Physics, 1994.

[24] Boris Katsnelson, Valery Petnikov, and James Lynch. *Fundamentals of Shallow Water Acoustics*. Springer, 2012.

[25] M. D. Vera. *Computational Methods for Physical Systems*. The University of Southern Mississippi, 2010.

[26] R.H. Hardin and F.D. Tappert. Applications of the split-step fourier method to the numerical solution of nonlinear and variable coefficient wave equations. volume 15.

[27] A. Bamberger, B. Engquist, L. Halpern, and P. Joly. Higher order parabolic wave equation approximations in heterogeneous media. *Journal of Applied Mathematics*, 48.

[28] M.D. Collins. Applications and time-domain solution of higher-order parabolic equations in underwater acoustics. *Journal of the Acoustical Society of America*, 86.

[29] M.D. Collins. A higher-order parabolic equation for wave propagation in an ocean overlying an elastic bottom. *Journal of the Acoustical Society of America*, 86.

[30] B.T.R. Wetton and G.H. Brooke. One-way wave equations for seismo-acoustic propagation in elastic waveguides. *Journal of the Acoustical Society of America*, 87.

[31] Michael D. Collins. Generalization of the split-step Padé solution. *Journal of the Acoustical Society of America*, 96:382–385, 1994.

[32] Vera M. D. Complex-density, equivalent-fluid modeling of acoustic interaction with the seafloor. volume 2, page 6. Acoustical Society of America, 2008.

[33] Steven Kirkup. Finding the limitations of the expanded equivalent fluid approximation for simulating acoustic interactions with the ocean bottom. The University of Southern Mississippi Honors Thesis, May 2013. Undergraduate Thesis.

[34] Michael D. Collins. Higher-order Padé approximations for accurate and stable elastic parabolic equations with application to interface wave propagation. *Journal of the Acoustical Society of America*, 89:1050–1057, 1991.

[35] Jack Caldwell and William Dragoset. A brief overview of seismic air-gun arrays. *The Leading Edge*, 19:898–902, August 2000.

[36] Stephens, 2012. personal communication.

[37] Bill Dragoset. Introduction to air guns and air-gun arrays. *The Leading Edge*, 19:892–897, August 2000.

[38] P. Worcester and R. Spindel. North Pacific Acoustic Laboratory. *Journal of the Acoustical Society of America*, 117:1499–1510, 2005.